THE ASTROPHYSICAL JOURNAL, 317:62–81, 1987 June 1


# DYNAMICS OF THE OUTER DISK AND HALO OF M31

RICHARD NOLTHENIUS[1]
Steward Observatory and University of California, Los Angeles
AND
HOLLAND C. FORD
Space Telescope Science Institute, Department of Physics and Astronomy, Johns Hopkins University; and University of California, Los Angeles
*Received 1986 February 18; accepted 1986 November 6*

## ABSTRACT

We present observations of 37 planetary nebulae projecting 15–30 kpc radius near the major axis on both the southwest and northeast sides of M31. We give velocities for 34 of the nebulae, separate them into disk and halo objects, and analyze them using four published models of M31's warped disk. We prefer the Newton-Emerson model.

The disk planetaries are consistent with a constant planetary nebula/disk mass ratio, with scale length 4.6 kpc. The number of planetaries per solar mass is $2.4 \times 10^{-8}$, about one-fourth of the solar neighborhood value. The (assumed flat) rotation rate is about $218 \pm 12$ km s$^{-1}$, $\sim 12$ km s$^{-1}$ below the circular velocity. A least-squares procedure gives the $r$ and $\theta$ velocity dispersions, the latter being about $38 \pm 12$ km s$^{-1}$ for all models. We use simple models to infer a $Z$ dispersion, which indicates that the planetaries form a disk of semithickness 1–3 kpc. The total disk population is probably 2700 or more.

The rotation rate and dispersion of the halo planetaries are $92 \pm 43$ km s$^{-1}$ and $116 \pm 48$ km s$^{-1}$, respectively, in good agreement with the globular cluster system. None of the planetaries belong to known globular clusters. The total spheroidal planetary nebula population is about $6500 \pm 3500$, 2–6 times the Milky Way value, and suggests that M31 has a more massive spheroid. The total planetary nebula population is about 1–2 times that of the Galaxy.

*Subject headings:* galaxies: individual (M31) — galaxies: internal motions — galaxies: structure — nebulae: planetary

## I. INTRODUCTION

Planetary nebulae are an ideal probe of the dynamics of Population II stars in nearby galaxies. They can be readily identified using narrow-band filters, and their emission lines can provide accurate line-of-sight velocities with a minimum of telescope time. Papers in this series have used planetary nebulae to study old stellar populations, the stellar death rate, and dynamics of nearby galaxies.

A number of important questions about how galaxies form and evolve can best be addressed with information from the outermost regions. Among these are: How does the thickness of the stellar disk vary with radius? In the inner regions (<4–5 scale lengths) it appears constant (van der Kruit and Searle 1981*a*, *b*, 1982*a*, *b*). Is there a "thick disk" component in spirals (Wyse and Jones 1983) as there seems to be in S0 galaxies (Burstein 1979)? The planetary nebula sample presented here extends to $\sim 6$ radial scale lengths and, with simple assumptions, can be used to infer a planetary nebula disk thickness. What is the dynamical state of the field halo stars, and is it similar to that for globular clusters? A high line-of-sight velocity dispersion would argue against highly radial orbits. The planetary-to-mass ratio is much lower in the halo of our Galaxy than in the disk. Is this true of M31 as well? From the space distribution in the disk and halo it is possible to estimate the total disk and halo planetary nebula populations.

[1] Present address: Board of Studies in Astronomy and Astrophysics, University of California, Santa Cruz, CA 95064

Previous papers in this series have presented identifications of planetaries in the inner disk and bulge of M31 and estimated stellar death rates and the total planetary nebula population (Ford and Jacoby 1978*a*, hereafter Paper V; Ford and Jacoby 1978*b*, hereafter Paper VIII). Lawrie and Ford (1982, herafter Paper IX) made a similar study after obtaining a deeper sample near the center.

We complement these studies by presenting here observations and analysis of 37 planetaries at sky-projected distances of 15–30 kpc from the center (hereafter, the distance to M31 is assumed to be 690 kpc [van den Bergh 1969]). We begin by separating these into probable disk and probable halo objects. We analyze the disk members using four published warp models, finding the rotation rate and velocity dispersions in the radial and azimuthal directions and the distribution in radius. We combine the dispersions with simple models to estimate the thickness of the stellar disk beyond 15 kpc. Finally, we estimate the total disk population of planetary nebulae.

The treatment for the halo will be similar. First, we find the distribution in space, then use this to decompose the velocities into rotational and random components. These results will be compared with those for the globular cluster system and the bulge. We then estimate the total spheroidal population of planetaries and the planetary–to–globular cluster ratio.

The total sample planetary-to-mass and planetary-to-luminosity ratios will then be found and combined with the nuclear results to estimate the total population and to compare this with the Milky Way and current theory.

TABLE 1

PLATE-FILTER COMBINATIONS FOR M31 DISK AND HALO SURVEY

| Filter | $\lambda_c$/FWHM (Å) | Transmission (%) | Size (cm) | Emulsion | Nominal Exposure Time (minutes) |
|---|---|---|---|---|---|
| $\lambda$5000 interference filter ........... | 5015/32[a] | 50[a] | 14.0 diameter | 70% $H_2$-soaked IIIa-J or IIIa-F | 120 |
| GG 475 on-band .................. | 5100/500 | 90 | 16.5 × 16.5 | 70% $H_2$-soaked IIIa-J | 60 |
| OG 5 off-band .................... | 5900/1000 | 91 | 20.3 × 25.4 | $N_2$-baked IIa-D | 3/60 |

[a] The central wavelength, bandpass, and transmission were measured by Jacoby 1980 in an f/2.8 beam which simulated the Mayall 4 m telescope prime focus.

## II. OBSERVATIONS

### a) Identifications

The M31 survey fields were photographed by H. Ford and D. Jenner on 1978 September 23, 24, 25, and 26 with the Mayall 4 m telescope's f/2.7 prime-focus camera and UBK-7 corrector. Table 1 lists the plate-filter combinations which were used to find planetary nebulae in the disk and halo by isolating the [O III] $\lambda$5007 emission line. The IIIa-J and IIIa-F plates were sensitized by soaking in a 70% hydrogen mixture. The IIa-D plates were sensitized by baking 4 hr at 60° C in nitrogen gas. Because of M31's rotation and $-300$ km s$^{-1}$ systemic velocity, the $\lambda$5007 interference filter, which was optimized for Jacoby's (1980) survey of the Large Magellanic Cloud, could be used only on the northeast side of M31. Consequently, the interference filter was used to photograph the northeast side of M31 while a first-quarter Moon was up, and the GG 475 on-band filter was used to photograph the southwest side of M31 after the Moon had set. Although the planetary nebulae were somewhat more difficult to identify on the plates taken with the GG 475 filter than on those taken with the interference filter, the former were superior because they reached a slightly fainter limiting magnitude and covered a larger area. Table 2 summarizes the characteristics and plate centers of the on-band photographs.

The on-band off-band plate pairs were blinked on the KPNO Gaertner blink comparator by E. Eason. Approximately 6 hr were required to blink each pair of plates. In order to avoid overlooking nebulae because of fatigue, only one plate pair was blinked each day. Every image that blinked on the on-band plate and that was not obviously a dust speck was noted. Subsequently, all such images and the corresponding off-band fields were inspected with a low-power magnifying glass. Of the original 51 candidates, 13 were rejected either because they did not have a stellar image profile or because the image could not be recovered on the on-band plate. One of the remaining 38 candidates was reclassified as an H II region (BA 685; Baade and Arp 1964). The remaining 37 candidates are listed in Table 3; 34 of these were confirmed as planetary nebulae by the spectroscopic observations discussed in § II*b*. Their positions, together with the plate field boundaries, are shown in Figure 1. We rechecked the coordinates and images of the three nebulae (M31-352, M31-354, and M31-358) which could not be found with the intensified image dissector-scanner (IIDS) spectrograph. One nebula (M31–358) was missed because erroneous coordinates were used at the telescope. All three nebulae appear to be real, and we have included them in Table 3.

Equatorial coordinates for the planetary nebulae are given in Table 3. The designations given in the first column of Table 3 follow the numbering sequence in Ford and Jacoby's (1978*b*) catalog of planetary nebulae in M31. Eight of the planetary nebulae, which are marked with an asterisk in Table 3, have radial velocities which show that they would be in retrograde orbits if they were in M31's disk. Because a large fraction of retrograde orbits is not expected in a flattened rotating disk, these nebulae almost certainly belong to M31's halo population. Coordinates for the nebulae and nearby reference stars were derived by using a KPNO glass copy of the Palomar Sky Survey to transform positions measured on the 4 m plates to the AGK3. The technique is described in detail by Ford and Jenner (1975). We estimate that the accuracy of the planetary positions relative to the reference stars is better than 1″. In order to facilitate future observations of these faint nebulae, we

TABLE 2

M31 ON-BAND DISK AND HALO SURVEY PLATES

| KPNO PF[a] Plate Number | Field | Filter | Emulsion | Exposure Time (minutes) | Seeing | R.A.(1975.0) | Decl.(1975.0) |
|---|---|---|---|---|---|---|---|
| 2893................. | SW 1 | GG 475 | IIIa-J | 60 | 3″–4″ | $0^h36^m.863$ | 39°48′.37 |
| 2895................. | SW 2 | GG 475 | IIIa-J | 60 | 3 | 34.391 | 39 01.84 |
| 2901................. | SW 3 | GG 475 | IIIa-J | 75 | 3 | 41.005 | 39 31.47 |
| 2908................. | SW 4 | GG 475 | IIIa-J | 75 | 2 | 33.096 | 40 22.94 |
| 2888................. | NE 1 | 5015 | IIIa-J | ... | ... | 49.686 | 42 51.02 |
| 2911................. | NE 1–2 | GG 475 | IIIa-J | 75 | 2 | 49.307 | 42 56.58 |
| 2897................. | NE 2 | 5015 | IIIa-F | 135 | 3 | 51.666 | 43 15.87 |
| 2905................. | NE 5 | 5015 | IIIa-F | 120 | 1 | 48.510 | 42 11.29 |
| 2907................. | NE 6 | 5015 | IIIa-F | 110 | 2 | 45.491 | 42 35.74 |
| 2899................. | NE 7 | 5015 | IIIa-F | 115 | 3–4 | 53.488 | 43 41.62 |

[a] Prime focus.

TABLE 3

Coordinates of Remote Disk and Halo Planetary Nebulae in M31

| Number[a] | R.A.(1975.0) | Decl.(1975.0) |
|---|---|---|
| 335 | 00h36m21s.61 | 39°44′21″.1 |
| 336 | 36 17.48 | 39 41 49.0 |
| 337 | 35 59.81 | 39 42 35.9 |
| 338 | 36 33.54 | 39 51 58.6 |
| 339 | 38 02.89 | 39 58 48.0 |
| 340 | 37 47.70 | 40 03 06.4 |
| 341 | 37 44.97 | 40 06 45.4 |
| 342 | 38 24.46 | 40 02 48.7 |
| 343 | 37 56.87 | 40 01 05.6 |
| 344 | 38 52.19 | 40 02 12.6 |
| 345 | 38 32.58 | 39 42 46.1 |
| 346 | 36 40.77 | 40 06 54.4 |
| 347 | 36 23.20 | 39 58 54.8 |
| 348 | 36 18.60 | 40 00 36.4 |
| 349 | 37 41.92 | 39 37 44.1 |
| 350 | 33 48.16 | 39 20 09.4 |
| 351 | 34 38.97 | 39 21 17.6 |
| 352[b] | 35 27.14 | 39 16 30.2 |
| 353* | 39 58.62 | 39 19 57.4 |
| 354[b] | 40 49.18 | 39 31 54.0 |
| 355* | 40 16.31 | 39 46 46.8 |
| 356 | 39 21.63 | 39 48 48.7 |
| 357* | 32 30.10 | 40 21 25.6 |
| 358[b] | 34 38.66 | 40 42 16.7 |
| 359* | 34 34.40 | 40 23 10.6 |
| 360* | 34 44.16 | 40 22 06.4 |
| 361 | 47 30.75 | 42 41 44.0 |
| 362* | 50 36.30 | 42 55 15.0 |
| 363 | 45 36.23 | 42 29 47.0 |
| 364 | 46 40.32 | 42 28 27.3 |
| 365 | 44 50.89 | 42 32 17.1 |
| 366* | 45 03.48 | 42 52 31.0 |
| 367 | 45 37.65 | 42 50 43.8 |
| 368 | 44 29.92 | 42 28 41.3 |
| 369 | 45 48.86 | 42 22 36.1 |
| 370 | 46 35.37 | 42 51 55.5 |
| 371* | 44 19.70 | 42 47 14.2 |

[a] An asterisk following the number indicates a halo planetary nebula.

[b] A nebula which could not be found with the IIDS on the 4 m telescope. M31-358 was missed because of an error in the coordinates which were used during the observing run.

have listed in Table 4 the positions of three close reference stars for each nebula. The three reference stars are listed in order of apparent $\lambda$5007 brightness, and the star which was used for a successful blind offset with the IIDS spectrograph is marked with an asterisk.

### *b) Radial Velocity Measurements*

We measured the radial velocities of 34 nebulae with the IIDS and "gold" spectrograph on the Mayall 4 m telescope. The observations were made with a pair of 3″.2 apertures and an 830 line mm$^{-1}$ grating used in the second order, which gave a reciprocal dispersion of 34 Å mm$^{-1}$ or 0.68 per channel. The nebulae, which were centered by using a raster scan of 1 minute integrations to maximize the signal, were observed in the west aperture only. Because M31's surface brightness is low at $R \geq 20$ kpc and the sky is faint in the spectral region near 5000 Å, we did not increase the noise in our spectra by subtracting the sky.

The centroids of H$\beta$ ($\lambda$4861.33), [O II] $\lambda$4959 ($\lambda$4958.92), and [O III] $\lambda$5007 ($\lambda$5006.85) were converted to observed wavelengths by using a cubic polynomial fit to seven helium and argon lines ($\lambda\lambda$4806.070, 4847.900, 4879.900, 4921.930, 4965.120, 5015.675, and 5047.736) in a comparison spectrum taken immediately after the observation of the nebula. The rms residual of the polynomial fit was typically $\sim$0.1 Å. Because systematic errors are often larger than internal errors, each night we observed two semistellar Galactic planetary nebula radial velocity standards, M1-2 and VY 2-3. These observations are summarized in Table 5, which includes the Lick Observatory image-tube scanner (ITS) radial velocities previously adopted by Ford, Jacoby, and Jenner (1977, hereafter FJJ) and those recently published by Schneider *et al.* (1983).

It is clear from the IIDS velocities of the M31 planetaries (cf. Table 6) that there are small but statistically significant differences between the $\lambda$5007 velocities and the velocities derived from H$\beta$ ($\Delta v = -5.7$ km s$^{-1}$) and $\lambda$4959 ($\Delta v = -10.8$ km s$^{-1}$) (cf. § II*c*). There are two reasons why we chose to derive these systematic corrections from the M31 data rather than from the observations of VY 2-3 and M1-2. First, it appears that the H$\beta$ velocities in the two Galactic nebulae are physically different from the [O III] velocities (cf. Nolthenius and Ford 1986).

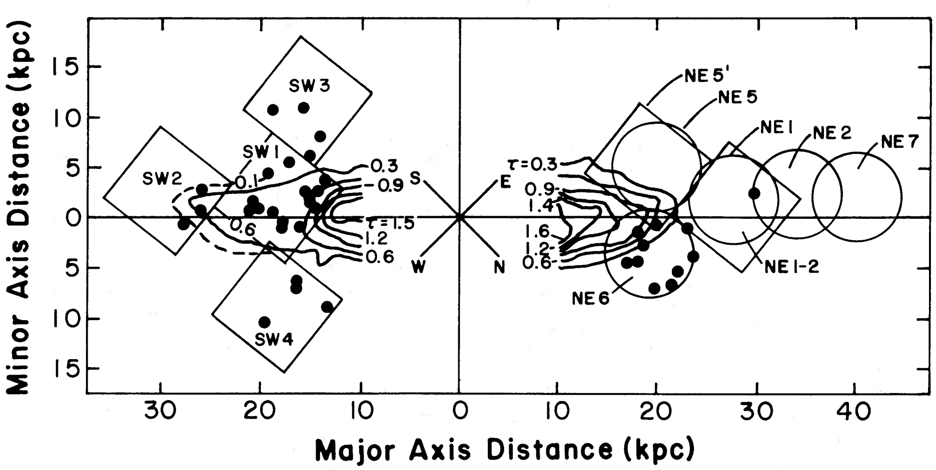


FIG. 1.—Plate field coverage, planetary nebula location, and $\lambda$5007 optical depth contours. The $x$-axis is oriented along P.A. = 38°; the assumed distance is 690 kpc.

TABLE 4

REFERENCE STAR COORDINATES FOR PLANETARY NEBULAE IN M31

| Star[a] | R.A.(1975.0) | Decl.(1975.0) |
|---|---|---|
| 335: | | |
| 1* ......... | 00h36m22s.11 | 39°42′48″.0 |
| 2 .......... | 36 27.53 | 39 42 49.9 |
| 3 .......... | 36 22.22 | 39 44 49.9 |
| 336: | | |
| 1* ......... | 36 17.48 | 39 40 47.4 |
| 2 .......... | 36 16.16 | 39 42 50.6 |
| 3 .......... | 36 19.20 | 39 40 56.0 |
| 337: | | |
| 1 .......... | 36 01.16 | 39 44 13.9 |
| 2* ......... | 36 02.87 | 39 41 32.1 |
| 3 .......... | 35 51.24 | 39 42 02.0 |
| 338: | | |
| 1 .......... | 36 34.98 | 39 51 13.7 |
| 2 .......... | 36 32.07 | 39 53 31.2 |
| 3* ......... | 36 29.24 | 39 52 12.1 |
| 339: | | |
| 1* ......... | 37 59.34 | 39 58 17.2 |
| 2 .......... | 38 13.02 | 39 58 38.2 |
| 3 .......... | 38 02.49 | 39 57 50.3 |
| 340: | | |
| 1* ......... | 37 50.74 | 40 03 21.9 |
| 2 .......... | 37 37.61 | 40 03 02.1 |
| 3 .......... | 37 45.23 | 40 02 24.2 |
| 341: | | |
| 1 .......... | 37 48.32 | 40 08 00.4 |
| 2 .......... | 37 30.86 | 40 06 13.7 |
| 3* ......... | 37 45.01 | 40 07 01.7 |
| 342: | | |
| 1 .......... | 38 20.07 | 40 02 44.0 |
| 2* ......... | 38 25.49 | 40 02 21.5 |
| 3 .......... | 38 26.68 | 40 02 58.0 |
| 343: | | |
| 1 .......... | 37 50.71 | 40 03 22.4 |
| 2 .......... | 38 03.45 | 39 59 17.6 |
| 3* ......... | 37 55.84 | 40 00 28.0 |
| 344: | | |
| 1 .......... | 38 53.29 | 40 01 11.3 |
| 2* ......... | 38 53.24 | 40 02 17.8 |
| 3 .......... | 38 51.62 | 40 02 28.8 |
| 345: | | |
| 1 .......... | 38 34.50 | 39 41 53.9 |
| 2 .......... | 38 32.45 | 39 41 26.8 |
| 3* ......... | 38 31.35 | 39 42 52.1 |
| 346: | | |
| 1 .......... | 36 54.70 | 40 06 52.8 |
| 2 .......... | 36 48.70 | 40 08 29.3 |
| 3* ......... | 36 37.58 | 40 06 14.6 |
| 347: | | |
| 1* ......... | 36 23.68 | 39 58 31.6 |
| 2 .......... | 36 24.10 | 40 00 16.6 |
| 3 .......... | 36 16.96 | 39 59 07.4 |
| 348: | | |
| 1 .......... | 36 26.15 | 40 00 44.2 |
| 2 .......... | 36 15.40 | 39 59 59.2 |
| 3* ......... | 36 18.86 | 40 00 21.6 |
| 349: | | |
| 1* ......... | 37 37.81 | 39 38 13.2 |
| 2 .......... | 37 37.26 | 39 36 50.0 |
| 3 .......... | 37 46.95 | 39 37 21.6 |
| 350: | | |
| 1 .......... | 33 39.19 | 39 19 58.6 |
| 2 .......... | 33 49.70 | 39 18 26.7 |
| 3* ......... | 33 48.40 | 39 20 10.1 |
| 351: | | |
| 1 .......... | 34 40.18 | 39 20 27.5 |
| 2* ......... | 34 36.75 | 39 21 27.8 |
| 3 .......... | 34 39.55 | 39 21 07.9 |
| 352: | | |
| 1 .......... | 35 20.10 | 39 16 43.2 |
| 2 .......... | 35 28.61 | 39 16 43.6 |
| 3 .......... | 35 29.40 | 39 16 19.2 |
| 353: | | |
| 1* ......... | 39 59.22 | 39 20 53.3 |
| 2 .......... | 40 04.19 | 39 18 54.2 |
| 3 .......... | 39 54.86 | 39 19 56.2 |
| 354: | | |
| 1 .......... | 00h40m52s.00 | 39°32′32″.3 |
| 2 .......... | 40 50.75 | 39 31 01.6 |
| 3 .......... | 40 47.57 | 39 32 46.3 |
| 355: | | |
| 1 .......... | 40 27.24 | 39 47 19.8 |
| 2 .......... | 40 15.74 | 39 45 33.5 |
| 3* ......... | 40 15.50 | 39 46 10.7 |
| 356: | | |
| 1* ......... | 39 18.79 | 39 49 08.4 |
| 2 .......... | 39 27.31 | 39 49 32.0 |
| 3 .......... | 39 19.58 | 39 49 23.6 |
| 357: | | |
| 1 .......... | 32 34.58 | 40 21 29.1 |
| 2 .......... | 32 21.32 | 40 22 08.2 |
| 3* ......... | 32 32.21 | 40 21 55.3 |
| 358: | | |
| 1 .......... | 34 31.95 | 40 41 28.9 |
| 2 .......... | 34 40.82 | 40 41 02.5 |
| 3 .......... | 34 36.92 | 40 42 37.1 |
| 359: | | |
| 1* ......... | 34 32.95 | 40 23 59.6 |
| 2 .......... | 34 33.10 | 40 24 29.6 |
| 3 .......... | 34 37.86 | 40 22 45.4 |
| 360: | | |
| 1 .......... | 34 45.72 | 40 21 22.8 |
| 2 .......... | 34 54.61 | 40 21 44.7 |
| 3* ......... | 34 42.37 | 40 21 52.9 |
| 361: | | |
| 1 .......... | 47 39.66 | 42 42 59.4 |
| 2 .......... | 47 23.91 | 42 42 40.6 |
| 3* ......... | 47 31.25 | 42 41 03.9 |
| 362: | | |
| 1 .......... | 50 32.62 | 42 54 47.7 |
| 2* ......... | 50 36.90 | 42 55 48.1 |
| 3 .......... | 50 33.99 | 42 55 49.3 |
| 363: | | |
| 1 .......... | 45 59.53 | 42 29 03.2 |
| 2 .......... | 45 57.98 | 42 28 06.4 |
| 3* ......... | 45 31.27 | 42 29 19.9 |
| 364: | | |
| 1 .......... | 46 58.47 | 42 26 26.2 |
| 2* ......... | 46 43.71 | 42 27 15.6 |
| 3 .......... | 47 04.83 | 42 27 18.4 |
| 365: | | |
| 1* ......... | 44 48.60 | 42 34 49.3 |
| 2 .......... | 45 00.03 | 42 31 42.5 |
| 3 .......... | 44 50.80 | 42 29 51.1 |
| 366: | | |
| 1 .......... | 45 09.37 | 42 52 29.8 |
| 2* ......... | 45 03.78 | 42 52 10.8 |
| 3 .......... | 45 13.31 | 42 50 12.0 |
| 367: | | |
| 1* ......... | 45 40.01 | 42 51 28.7 |
| 2 .......... | 45 34.20 | 42 51 37.3 |
| 3 .......... | 45 23.16 | 42 49 49.5 |
| 368: | | |
| 1 .......... | 44 34.62 | 42 26 01.4 |
| 2 .......... | 44 33.09 | 42 30 06.6 |
| 3* ......... | 44 29.88 | 42 29 01.0 |
| 369: | | |
| 1 .......... | 45 33.77 | 42 22 31.4 |
| 2 .......... | 45 59.52 | 42 20 10.3 |
| 3* ......... | 45 48.87 | 42 22 21.6 |
| 370: | | |
| 1 .......... | 46 28.34 | 42 48 26.5 |
| 2* ......... | 46 42.02 | 42 49 45.1 |
| 3 .......... | 46 22.77 | 42 53 10.3 |
| 371: | | |
| 1 .......... | 44 34.77 | 42 48 32.3 |
| 2 .......... | 44 19.40 | 42 48 24.9 |
| 3 .......... | 44 18.16 | 42 46 28.8 |

[a] The star which was successfully used for a blind offset is marked with an asterisk in each case.

TABLE 5

Observed Heliocentric Velocities of Radial Velocity Standards

A. KPNO IIDS

| Nebula | Date 1979 | Emission Line | $v_{0,\mathrm{obs}}$ [a] (km $s^{-1}$) |
|---|---|---|---|
| VY 2-3......... | Sep 19/20 | Hβ | −49.0 |
| | | λ4959 | −52.4 |
| | | λ5007 | −53.2 |
| | Sep 20/21 | Hβ | −47.0 |
| | | λ4959 | −51.8 |
| | | λ5007 | −56.8 |
| | Sep 21/22 | Hβ | −43.1 |
| | | λ4959 | −53.7 |
| | | λ5007 | −54.2 |
| | Sep 22/23 | Hβ | −41.2 |
| | | λ4959 | −50.8 |
| | | λ5007 | −57.2 |
| M1-2........... | Sep 19/20 | Hβ | −7.1 |
| | | λ4959 | −24.3 |
| | | λ5007 | −26.2 |
| | Sep 20/21 | Hβ | −11.3 |
| | | λ4959 | −25.5 |
| | | λ5007 | −29.9 |
| | Sep 21/22 | Hβ | −8.7 |
| | | λ4959 | −20.7 |
| | | λ5007 | −24.2 |
| | Sep 22/23 | Hβ | −15.4 |
| | | λ4959 | −30.8 |
| | | λ5007 | −33.4 |

B. Comparisons with Previous Work

| Nebula | Emission Line | KPNO Mean Velocity (km $s^{-1}$) | $v_0$ FJJ[b] | $v_0$ STPP[c] |
|---|---|---|---|---|
| VY 2-3........... | Hβ | −45.1 | ... | ... |
| | λλ4959, 5007 | −53.8 | −43.5 | −49.6 |
| M1-2............. | Hβ | −10.6 | ... | ... |
| | λλ4959, 5007 | −26.9 | −17.6 | −10.7 |

C. Lick ITS

| Nebula | Date 1975 | Emission Line | $v_{0,\mathrm{obs}}$ (km $s^{-1}$) |
|---|---|---|---|
| M1-2............. | Oct 4 | Hβ | 1.8 |
| | | λ4959 | −21.5 |
| | | λ5007 | −26.9 |
| M1-2............. | Oct 5 | Hβ | −3.1 |
| | | λ4959 | −27.0 |
| | | λ5007 | −32.2 |

[a] A −10.6 km $s^{-1}$ correction has been added to the λ4959 observed velocity, as explained in the text.

[b] Ford, Jacoby, and Jenner 1977.

[c] Schneider *et al.* 1983.

Second, there could be small systematic differences between the measured positions of the bright lines in the two Galactic planetaries and the weak lines in the M31 planetaries. Consequently, we have used the internal corrections derived from the faint nebulae in the next section and corrected the IIDS λ4959 velocities in Tables 5 and 6 by adding −10.8 km $s^{-1}$.

The mean difference between the IIDS [O III] λλ4959, 5007 velocities in Table 5 and the Lick ITS velocities adopted by FJJ is +10.4 km $s^{-1}$. However, we found that adding the +10.4 km $s^{-1}$ correction to the observed radial velocities reduced the agreement of our derived M31 systemic velocity with other accurately measured values. Consequently, we have not corrected the IIDS velocities to the Lick ITS system by adding +10.4 km $s^{-1}$. We estimate that the uncertainty in the true zero point of the IIDS velocities is ~ ±5 km $s^{-1}$.

### c) *Defining the Adopted Velocities*

The planetaries span 4° across the sky, large enough that the contribution of the Sun's Galactic motion may be significantly different for different planetaries. Fortunately, these corrections were small (most less than 1 km $s^{-1}$) because of the orientation of the major axis, and have been ignored. Each of the three emission lines (Hβ, λ4959, and [O III] λ5007) were measured, giving three velocities for each planetary.

The error in a velocity is dominated by the resolution, which was 0.62 Å $\mathrm{channel}^{-1}$. The residual wavelength calibration error was 0.15 channel, giving an error of 6–7 km $s^{-1}$ for all lines. Before combining each line's velocity into an adopted velocity for the planetary, we derived corrections to all Hβ and λ4959 velocities of −5.7 km $s^{-1}$ and −10.8 km $s^{-1}$, respectively. This put all lines on a common standard, that of the stronger λ5007 line. Formally, three independent line velocities with errors of 6–7 km $s^{-1}$ give a net planetary nebula velocity error of $\sigma = 4$ km $s^{-1}$. However, the true uncertainty is almost certainly higher than this formal error, especially when possible systematic errors are considered. We conservatively adopt 10 km $s^{-1}$ for the standard 1 $\sigma$ error of all of Table 6, column (7), velocities.

### d) *Radial Velocities of Planetary Nebulae That Project near M31's Minor Axis*

During the 1975 and 1979 observing seasons we measured the radial velocities of 25 planetary nebulae in M31 which, with four exceptions, project near the minor axis. Because of M31's high inclination the velocities of these nebulae are not suitable for the analysis to follow, and have not been included. Nonetheless, the velocities are apparently characteristic of the velocity dispersion in the bulge and inner halo, and are presented here because they may prove interesting for future kinematical and chemical abundance studies.

#### i) *Kitt Peak IIDS Radial Velocities*

The Kitt Peak IIDS observations were made in 1979 and were interspersed with the observations of nebulae in the outer disk and halo. The reductions, velocity corrections, and weights were the same as those described in §§ II*b* and II*c*. Many of the nebulae project onto the bright bulge of M31 and thus show an underlying stellar continuum. In such cases the weak Hβ emission line often was unmeasurable when superposed on the underlying Hβ absorption line. Because the [O III] lines carry most of the velocity information in these faint high-excitation nebulae, the loss of Hβ does not significantly degrade the measured radial velocity. The observed and weighted heliocentric IIDS velocities are given in Table 7A. Positions and finding charts for the nebulae can be found in Ford and Jacoby (1978*b*) using the designations in the first column.

#### ii) *Lick ITS Radial Velocities*

The Lick radial velocities were measured with the image-tube scanner (ITS; Robinson and Wampler 1972, 1973) using the Lick Cassegrain spectrograph (Miller, Robinson, and

TABLE 6

KPNO OBSERVATIONS[a]

| Object (1) | Date 1979 (2) | Integration Time (s) (3) | Line (4) | Peak Counts (5) | $V_{obs}$ (6) | $V_{adopted}$ (7) |
|---|---|---|---|---|---|---|
| 335...... | Sep 21 | 1560 | Hβ | 45 | −480.1 | −453.7 |
| | | | λ4959 | 275 | −449.6 | |
| | | | λ5007 | 900 | −458.6 | |
| 336...... | Sep 21 | 960 | Hβ | 75 | −496.3 | −488.2 |
| | | | λ4959 | 325 | −489.0 | |
| | | | λ5007 | 1100 | −498.9 | |
| 337...... | Sep 21 | 1560 | Hβ | 75 | −570.4 | −547.6 |
| | | | λ4959 | 200 | −541.7 | |
| | | | λ5007 | 550 | −553.9 | |
| 338...... | Sep 23 | 720 | Hβ | 60 | −415.3 | −427.6 |
| | | | λ4959 | 100 | −434.5 | |
| | | | λ5007 | 325 | −445.5 | |
| 339...... | Sep 22 | 1080 | Hβ | 40 | −454.6 | −424.9 |
| | | | λ4959 | 125 | −421.7 | |
| | | | λ5007 | 300 | −425.6 | |
| 340...... | Sep 22 | 720 | Hβ | 25 | −451.8 | −444.4 |
| | | | λ4959 | 175 | −446.5 | |
| | | | λ5007 | 475 | −453.9 | |
| 341...... | Sep 23 | 480 | Hβ | 20 | −558.1 | −557.7 |
| | | | λ4959 | 125 | −555.1 | |
| | | | λ5007 | 375 | −573.3 | |
| 342...... | Sep 23 | 1200 | Hβ | 75 | −458.7 | −440.4 |
| | | | λ4959 | 150 | −439.7 | |
| | | | λ5007 | 525 | −443.1 | |
| 343...... | Sep 24 | 720 | Hβ | 30 | −414.1 | −408.9 |
| | | | λ4959 | 250 | −407.9 | |
| | | | λ5007 | 525 | −420.3 | |
| 344...... | Sep 23 | 960 | Hβ | 40 | −507.8 | −506.8 |
| | | | λ4959 | 150 | −511.1 | |
| | | | λ5007 | 500 | −517.0 | |
| 345...... | Sep 23 | 720 | Hβ | 30 | −532.4 | −508.9 |
| | | | λ4959 | 175 | −507.2 | |
| | | | λ5007 | 500 | −512.9 | |
| 346...... | Sep 24 | 480 | Hβ | 30 | −476.4 | −463.5 |
| | | | λ4959 | 160 | −460.1 | |
| | | | λ5007 | 500 | −473.2 | |
| 347...... | Sep 24 | 720 | Hβ | 50 | −545.7 | −550.0 |
| | | | λ4959 | 225 | −553.2 | |
| | | | λ5007 | 650 | −563.3 | |
| 348...... | Sep 24 | 840 | Hβ | 90 | −509.2 | −501.5 |
| | | | λ4959 | 110 | −509.5 | |
| | | | λ5007 | 300 | −503.3 | |
| 349...... | Sep 21 | 720 | Hβ | 40 | −488.9 | −496.8 |
| | | | λ4959 | 150 | −502.7 | |
| | | | λ5007 | 500 | −512.5 | |
| 350...... | Sep 20 | 1020 | Hβ | 90 | −473.9 | −461.8 |
| | | | λ4959 | 300 | −459.5 | |
| | | | λ5007 | 825 | −473.2 | |
| 351...... | Sep 20 | 480 | Hβ | 80 | −476.0 | −465.9 |
| | | | λ4959 | 325 | −469.0 | |
| | | | λ5007 | 1050 | −473.9 | |
| 353...... | Sep 20 | 540 | Hβ | 40 | −273.3 | −262.9 |
| | | | λ4959 | 275 | −263.9 | |
| | | | λ5007 | 750 | −273.2 | |
| 355...... | Sep 23 | 1440 | Hβ | 45 | −416.9 | −407.2 |
| | | | λ4959 | 175 | −398.3 | |
| | | | λ5007 | 500 | −423.8 | |
| 356...... | Sep 23 | 720 | Hβ | 30 | −532.4 | −443.5 |
| | | | λ4959 | 175 | −507.2 | |
| | | | λ5007 | 500 | −512.9 | |
| 357...... | Sep 20 | 780 | Hβ | 70 | −358.8 | −348.8 |
| | | | λ4959 | 500 | −347.2 | |
| | | | λ5007 | 1100 | −361.5 | |
| 359...... | Sep 22 | 720 | Hβ | 30 | −530.3 | −511.1 |
| | | | λ4959 | 90 | −510.1 | |
| | | | λ5007 | 350 | −517.2 | |
| 360...... | Sep 23 | 1200 | Hβ | 30 | −290.5 | −262.6 |
| | | | λ4959 | 100 | −254.3 | |
| | | | λ5007 | 300 | −269.2 | |
| 361...... | Sep 20 | 1260 | Hβ | 120 | −87.4 | −84.9 |
| | | | λ4959 | 450 | −86.0 | |
| | | | λ5007 | 1100 | −103.3 | |
| 362...... | Sep 21 | 1440 | Hβ | 90 | −114.5 | −117.2 |
| | | | λ4959 | 275 | −123.9 | |
| | | | λ5007 | 900 | −133.2 | |
| | Sep 23 | 480 | Hβ | 650 | −78.8 | −76.5 |
| | | | λ4959 | 675 | −79.4 | |
| | | | λ5007 | 1900 | −91.8 | |
| 363...... | Sep 22 | 720 | Hβ | 55 | −96.9 | −94.7 |
| | | | λ4959 | 275 | −94.4 | |
| | | | λ5007 | 800 | −111.9 | |
| 364...... | Sep 22 | 960 | Hβ | 75 | −110.1 | −109.7 |
| | | | λ4959 | 275 | −110.9 | |
| | | | λ5007 | 775 | −127.2 | |
| 365...... | Sep 21 | 1440 | Hβ | 75 | −122.0 | −112.0 |
| | | | λ4959 | 325 | −120.2 | |
| | | | λ5007 | 1050 | −124.2 | |
| 366...... | Sep 21 | 720 | Hβ | 75 | −443.2 | −452.3 |
| | | | λ4959 | 400 | −461.3 | |
| | | | λ5007 | 1200 | −470.0 | |
| 367...... | Sep 21 | 720 | Hβ | 86 | −82.7 | −79.4 |
| | | | λ4959 | 368 | −79.9 | |
| | | | λ5007 | 1036 | −96.5 | |
| 368...... | Sep 22 | 720 | Hβ | 100 | −186.5 | −176.9 |
| | | | λ4959 | 300 | −173.5 | |
| | | | λ5007 | 975 | −192.0 | |
| 369...... | Sep 23 | 960 | Hβ | 40 | −43.4 | −78.9 |
| | | | λ4959 | 150 | −99.3 | |
| | | | λ5007 | 475 | −98.2 | |
| 370...... | Sep 20 | 720 | Hβ | 120 | −97.1 | −87.2 |
| | | | λ4959 | 350 | −86.2 | |
| | | | λ5007 | 900 | −101.6 | |
| 371...... | Sep 21 | 960 | Hβ | 80 | −163.8 | −173.2 |
| | | | λ4959 | 350 | −176.8 | |
| | | | λ5007 | 1000 | −195.4 | |

[a] NE 6/1 is an H II region (BA 685; Baade and Arp 1964) and not included in our analysis. Its velocity is in good agreement with H I data.

TABLE 7

HELIOCENTRIC RADIAL VELOCITIES OF PLANETARY NEBULAE WHICH PROJECT NEAR M31'S MINOR AXIS

A. KPNO IIDS (1979)

| Nebula[a] (1) | Date (2) | Integration Time (s) (3) | Emission Line (4) | Peak Counts (5) | $v_{obs}$ (km s$^{-1}$) (6) | $v_0$ [b] (km s$^{-1}$) (7) |
|---|---|---|---|---|---|---|
| 91* | Sep 23 | 720 | λ4959<br>λ5007 | 140<br>500 | −196.2<br>−221.9 | −203.3 |
| 272 | Sep 24 | 1080 | λ4959<br>λ5007 | 125<br>300 | −262.2<br>−270.8 | −260.9 |
| 286 | Sep 24 | 720 | λ4959<br>λ5007 | 40<br>100 | −222.6<br>−204.0 | −207.4 |
| 289 | Sep 24 | 720 | λ4959<br>λ5007 | 150<br>450 | −115.2<br>−134.7 | −119.4 |
| 290* | Sep 24 | 720 | Hβ<br>λ4959<br>λ5007 | 50<br>180<br>475 | −664.3<br>−656.1<br>−662.8 | −655.3 |
| 303 | Sep 23 | 960 | λ4959<br>λ5007 | 140<br>375 | −413.2<br>−428.6 | −415.1 |
| 304 | Sep 23 | 720 | Hβ<br>λ4959<br>λ5007 | 45<br>125<br>400 | −375.1<br>−328.9<br>−337.2 | −334.9 |
| 307 | Sep 23 | 1440 | λ4959<br>λ5007 | 90<br>300 | −337.1<br>−348.9 | −337.2 |
| 308 | Sep 23 | 1560 | Hβ<br>λ4959<br>λ5007 | 40<br>225<br>650 | −313.0<br>−309.0<br>−319.8 | −308.1 |
| 309 | Sep 22 | 960 | Hβ<br>λ4959<br>λ5007 | 80<br>350<br>1000 | −312.9<br>−295.9<br>−312.8 | −303.9 |
| 310 | Sep 22 | 1920 | λ4959<br>λ5007 | 60<br>175 | −213.9<br>−217.6 | −209.9 |
| 311* | Sep 23 | 1440 | λ4959<br>λ5007 | 200<br>650 | −440.2<br>−452.6 | −440.2 |
| 312* | Sep 22 | 1440 | λ4959<br>λ5007 | 80<br>180 | −285.2<br>−283.0 | −277.9 |
| 315 | Sep 22 | 960 | λ4959<br>λ5007 | 60<br>150 | −310.5<br>−309.5 | −303.8 |

B. LICK ITS (1975)

| Nebula[a] (1) | Date (2) | Integration Time (s) (3) | Emission Line (4) | $v_{obs}$ (km s$^{-1}$) (5) | $v_0$ [c] (km s$^{-1}$) (6) |
|---|---|---|---|---|---|
| 36* | Oct 4 | 1440 | λ4959<br>λ5007 | −111.9<br>−128.6 | −118.7 |
| 41 | Oct 5 | 1440 | λ4959<br>λ5007 | −477.7<br>−482.3 | −478.5 |
| 42 | Oct 4 | 960 | λ4959<br>λ5007 | −366.9<br>−389.5 | −376.7 |
| 43* | Oct 5 | 960 | λ4959<br>λ5007 | −61.6<br>−79.0 | −68.8 |
| 45* | Oct 4 | 960 | λ4959<br>λ5007 | −230.0<br>−250.2 | −238.5 |
| 46 | Oct 5 | 960 | λ4959<br>λ5007 | −425.3<br>−434.7 | −428.5 |
| 47* | Oct 5 | 960 | λ4959<br>λ5007 | −290.1<br>−303.1 | −295.1 |
| 49 | Oct 5 | 960 | λ4959<br>λ5007 | −343.9<br>−350.0 | −345.4 |
| 50* | Oct 5 | 1440 | λ4959<br>λ5007 | −294.1<br>−294.6 | −292.8 |
| 91* | Oct 4 | 960 | λ4959<br>λ5007 | −184.9<br>−205.0 | −193.4 |
| 295 | Oct 5 | 960 | λ4959<br>λ5007 | −321.6<br>−312.8 | −315.7 |
| 299 | Oct 4 | 960 | λ4959<br>λ5007 | −341.9<br>−326.0 | −332.4 |
| 304 | Oct 4 | 1440 | λ4959<br>λ5007 | −338.3<br>−358.8 | −347.0 |
| 308 | Oct 4 | 960 | λ4959<br>λ5007 | −328.1<br>−319.1 | −322.1 |
| 311* | Oct 5 | 1440 | λ4959<br>λ5007 | −397.0<br>−433.9 | −413.9 |

[a] An asterisk following the number indicates that the planetary nebula is a member of the bulge or halo.

[b] As explained in the text, a −5.1 km s$^{-1}$ correction was added to the Hβ velocity and a −10.6 km s$^{-1}$ correction was added to the λ4959 velocity. The mean heliocentric velocity was calculated from the observed velocities and the counts using eqs. (5) and (10).

[c] The mean heliocentric velocity was calculated by adding −10.3 km s$^{-1}$ to the λ4959 velocity, averaging the λ4959 and λ5007 velocities with equal weight, and adding the heliocentric correction.

Wampler 1976) on the Shane 3 m telescope. The [O III] $\lambda\lambda$4959, 5007 and H$\beta$ emission lines were observed by using an 830 line mm$^{-1}$ grating in the second order, which gave a central wavelength of $\sim$4700 Å and an effective dispersion of 56 Å mm$^{-1}$. A blind offset followed by a sequence of short integrations was used to find and maximize the signal from the faint nebulae (invisible with the TV acquisition system). The nebulae were "beam-switched" between a pair of 2″ apertures at 4 minute intervals using a L, R, R, L sequence. Small-scale spatial variations in the ITS response were removed by dividing a continuum source spectrum into the observed spectra. The left and right slits were summed independently and then sky-subtracted. Comparison spectra were taken immediately before and after the observations of each nebula. Because an adequate helium-argon comparison lamp was not available when the observations were made, only four comparison lines ($\lambda\lambda$4471.480, 4713.740, 4921.930, and 5015.680) could be used to derive the wavelength scale. A third-order polynomial was fitted to the eight comparison-line positions measured in the two bracketing spectra. The radial velocities from the left and right slits were then measured and averaged. Because the H$\lambda$ emission line always was weak and often unmeasurable, we excluded it from the velocity measurements.

ITS radial velocities for the Galactic planetary M1-2 were measured each night and are given in Table 5. Comparison of the ITS $\lambda\lambda$4959, 5007 mean velocity ($-26.9$ km s$^{-1}$ $\pm$ 2 km s$^{-1}$) with the IIDS mean velocity ($-26.9$ km s$^{-1}$) suggests that the Lick velocities are in the same system as the Kitt Peak velocities. Consequently, we have not applied an external correction to the Lick velocities.

The observed ITS velocities of the M31 planetary nebulae are given in Table 7B (col. [5]). There is a systematic difference ($-10.3$ km s$^{-1}$ $\pm$ 3.7 km s$^{-1}$) between the $\lambda$5007 velocity and the $\lambda$4959 velocity which is nearly identical with the IIDS difference. We computed the mean heliocentric velocity for the ITS velocities by adding $-10.3$ km s$^{-1}$ to the $\lambda$4959 velocity, averaging the $\lambda\lambda$4959 and 5007 velocities with equal weights, and adding the appropriate heliocentric correction. The heliocentric velocities are given in the last column of Table 7. As a final consistency check, we calculated the mean differences between the four nebulae (M31-91, M31-304, M31-308, and M31-311) measured with both instruments, obtaining a $-2.5$ km s$^{-1}$ difference with a 16.6 km s$^{-1}$ standard deviation. There appears to be no systematic difference between the two data sets.

After exclusion of the four nebulae in Table 7 which are not near the minor axis (M31-272, M31-286, M31-289, and M31-290), the mean velocity of the nebulae is $-308$ km s$^{-1}$ and the velocity dispersion is 95 km s$^{-1}$. This large velocity dispersion is, within the respective errors, equal to the 116 km s$^{-1}$ velocity dispersion for the planetary nebulae in the outer halo (cf. § VI*b*[ii]), and is comparable to the globular cluster velocity dispersion in the inner halo (130 km s$^{-1}$; Huchra, Stauffer, and Van Speybroeck 1982). In view of this, we conclude that the majority of these nebulae are members of the bulge or inner halo population rather than the disk. This conclusion is reinforced by comparing the observed radial velocities with the radial velocities of circular orbits in the disk at the projected positions of the nebulae. Seven of the 21 nebulae near the minor axis have velocities which would place them in retrograde orbits if they were in the disk. Consequently, these nebulae, which are marked with an asterisk in Table 7, must be in the bulge or halo.

## III. ANALYSIS AND RESULTS

### *a) Disk Planetaries*

#### i) *First Considerations*

With only sky-projected coordinates, there is no *a priori* way to know how the planetaries are distributed in space. They may belong to the disk, the halo, or both, or to an intermediate population. Van der Kruit and Searle (1981*a*, *b*, 1982*a*, *b*) find no evidence of intermediate populations in the edge-on disk galaxies they studied, and we will assume that the planetaries can be analyzed as if they belong to either a disk of small to moderate thickness or a nearly spherical halo.

The basic idea will be to find which planetaries have position and dynamics that are consistent with being disk objects and which halo objects. The neutral hydrogen disk in M31 extends out to at least 37 kpc (Haud 1981). The photometry of de Vaucouleurs (1958) shows that the stellar disk extends out to at least 25 kpc. Innanen *et al.* (1982) have digitally stacked together Palomar Schmidt plates and find a faint reddish continuum extending to 27 kpc on the southwest side. The most likely source is old Population II stars. It is reasonable to suppose that disk planetaries can be found out to the edge of M31's stellar disk, which, from the aforementioned work, appears to be between 25 and 30 kpc.

On the basis of the very small halo population of planetaries in the Milky Way, we expect the large majority of outer region planetaries which project to disk distances less than about 23 kpc to be members of the disk. With this background, we begin by projecting all 37 planetaries onto the disk to see whether the resulting dynamics are consistent with a disk population.

#### ii) *Disk Models*

The neutral hydrogen disk of M31 is well known to be warped. We consider here the models of Roberts and Whitehurst (1975), Henderson (1979) and Newton and Emerson (1977) as well as the flat disk model in analyzing the planetary nebulae. These follow the earlier work of Baade (1963), Arp (1964) and Roberts (1966). Other warp models are presented by Brinks and Burton (1984).

We adopted Roberts and Whitehurst's "drastically smoothed" warp model of the southwest side of M31 and assume that it is antisymmetric on the northeast side. We smoothly extrapolate their $i(y)$ curve beyond 33′ with a straight line. Henderson (1979) reinterpreted the Roberts-Whitehurst data in terms of an infinitely thin H I disk. We use Haud's (1981) slight modification of Henderson's disk. The Newton-Emerson model is not antisymmetric, and is less warped than the Henderson or Roberts-Whitehurst models. We assume that the inclination and the position angle (P.A.) of the major axis are constant beyond 30 kpc. The fourth model we consider is the standard flat disk model with P.A. = 38°, $i$ = 77°.

We regard the Newton-Emerson model as *a priori* the most reasonable, for the following reasons. High-resolution Cambridge aperture synthesis data (Emerson, cited in Whitehurst, Roberts, and Cram 1978) show an H I disk thickness varying between 0.5 kpc at 12 kpc to 2–3 kpc at 25 kpc. Roberts and Whitehurst (1975) and Whitehurst, Roberts, and Cram (1978) also find a thickness of 1.4 kpc as best explaining the observations. If M31's H I disk really has finite thickness, Henderson's model loses motivation. How to interpret the Roberts-Whitehurst model is unclear, since the position angle of the major axis varies in such a way that all positions within 30′ of the $x$-axis are very close to the "position angle of the major axis." The problems with this model are easiest to see when sky positions are projected onto the disk (Nolthenius 1984).

Deprojecting the sky coordinates onto these disk models is straightforward except for the Henderson and Newton-Emerson models, where shadowing can lead to multiple solutions. In these cases, we placed the planetary at the most probable position, assuming that the disk planetary nebula density falls off exponentially and that velocities are Gaussian about the circular velocity. In all cases, this leads to the smallest $r$ solution being adopted.

The disk coordinates of the planetaries for the four models are given in Table 8. Let the positions be measured in cylindrical coordinates, with the $z = 0$ plane the local plane of the galaxy, $r = 0$ the galactic center, and $\theta$ measured counterclockwise from the positive $x$-axis; $i$ is the inclination of the disk, described previously, and $\mu$ is the systemic velocity. For the $i$th planetary, let $v_{\theta_i}$ be the component of velocity in the $+\theta$ direction, $v_{r_i}$ the component in the $+r$ direction, $v_{z_i}$ the component in the $+z$ direction, and $\epsilon_i$ the measurement error. Then the observed line-of-sight planetary nebula velocity $v_i$ can be written

$$v_i = \mu + \alpha_i v_{\theta_i} + \beta_i v_{r_i} + \gamma_i v_{z_i} + \epsilon_i , \tag{1}$$

where

$$\alpha_i \equiv \cos\theta_i \sin i_i , \tag{2}$$

$$\beta_i \equiv \sin\theta_i \sin i_i , \tag{3}$$

$$\gamma_i \equiv \cos i_i . \tag{4}$$

All of the planetaries project to disk distances beyond 15 kpc, where we assume that the rotation curve is flat (Roberts and Whitehurst 1975; Haud 1981). The rotation rate of the planetaries can be found by taking the expectation of equation (1) along the $i$th line of sight. Assuming random errors, and no net $r$ or $z$ motion (consistent with the H I kinematics; Emerson and Newton 1978), the last three terms vanish. The expectation of $v_{\theta_i}$ is just the true rotation rate of the planetaries, $v_c^*$:

$$v_c^* = E(v_i/\alpha_i) - \mu . \tag{5}$$

TABLE 8

PROJECTED DISK POSITIONS AND CIRCULAR VELOCITIES OF M31 OUTER PLANETARIES

| | | Flat | | | Newton-Emerson | | | Roberts-Whitehurst | | | Henderson | | |
|---|---|---|---|---|---|---|---|---|---|---|---|---|---|
| Object | Field/Number | $r_d$ (kpc) | $\theta$ | $V_c$ (km s$^{-1}$) | $r_d$ (kpc) | $\theta$ | $V_c$ (km s$^{-1}$) | $r_d$ (kpc) | $\theta$ | $V_c$ (km s$^{-1}$) | $r_d$ (kpc) | $\theta$ | $V_c$ (km s$^{-1}$) |
| 335 | SW 1/1 | 20.9 | 166° | 164 | 21.5 | 161° | 168 | 20.3 | 179° | 159 | 21.1 | 164° | 164 |
| 336 | SW 1/2 | 21.6 | 164 | 202 | 22.3 | 159 | 207 | 20.8 | 179 | 194 | 21.9 | 161 | 203 |
| 337 | SW 1/3 | 21.3 | 172 | 258 | 21.7 | 167 | 261 | 21.1 | 179 | 255 | 21.4 | 171 | 257 |
| 338 | SW 1/4 | 19.0 | 172 | 133 | 19.3 | 167 | 135 | 18.8 | 179 | 132 | 19.0 | 172 | 133 |
| 339 | SW 1/5 | 19.1 | 145 | 158 | 20.4 | 140 | 169 | 16.4 | 165 | 134 | 19.2 | 144 | 159 |
| 340 | SW 1/6 | 16.7 | 157 | 163 | 17.5 | 151 | 170 | 15.5 | 171 | 151 | 16.3 | 159 | 161 |
| 341 | SW 1/7 | 15.4 | 164 | 276 | 15.9 | 158 | 285 | 14.9 | 175 | 266 | 15.2 | 167 | 276 |
| 342 | SW 1/8 | 18.6 | 141 | 187 | 20.0 | 136 | 201 | 15.5 | 161 | 154 | 18.4 | 142 | 185 |
| 343 | SW 1/A1 | 17.8 | 150 | 131 | 18.9 | 144 | 138 | 15.9 | 167 | 116 | 17.5 | 152 | 129 |
| 344 | SW 1/A2 | 21.1 | 131 | 322 | 22.9 | 127 | 351 | 15.8 | 155 | 238 | 43.0 | 251 | 644 |
| 345 | SW 1/A3 | 29.5 | 126 | 364 | 36.0H | 120 | 426 | 19.2 | 161 | 236 | 46.0 | 248 | 557 |
| 346 | SW 1/A5 | 16.9 | 196 | 175 | 16.6 | 192 | 172 | 16.6 | 191 | 173 | 16.7 | 194 | 175 |
| 347 | SW 1/A6 | 18.1 | 188 | 260 | 18.0 | 184 | 257 | 18.1 | 188 | 261 | 18.1 | 188 | 261 |
| 348 | SW 1/A7 | 18.2 | 193 | 213 | 18.0 | 190 | 210 | 18.0 | 189 | 212 | 18.2 | 193 | 213 |
| 349 | SW 1/B1 | 27.6 | 135 | 288 | 29.6 | 132 | 298 | 20.5 | 166 | 213 | 44.7 | 244 | 457 |
| 350 | SW 2/1 | 27.9 | 186 | 168 | 37.6H | 223 | 223 | 27.9 | 185 | 169 | 28.6 | 194 | 169 |
| 351 | SW 2/2 | 26.6 | 173 | 173 | 26.4 | 179 | 170 | 26.4 | 177 | 172 | 27.1 | 167 | 173 |
| 352 | SW 2/3 | ... | ... | ... | ... | ... | ... | ... | ... | ... | ... | ... | ... |
| 353 | SW 3/1 | 51.6H | 112 | −100 | 77.1H | 105 | −141 | 22.3 | 166 | −51 | 53.1 | 249 | −103 |
| 354 | SW 3/2 | ... | ... | ... | ... | ... | ... | ... | ... | ... | ... | ... | ... |
| 355 | SW 3/A1 | 38.4H | 112 | 296 | 57.2H | 105 | 414 | 17.8 | 154 | 140 | 49.4 | 253 | 376 |
| 356 | SW 3/A2 | 31.2 | 120 | 301 | 42.0H | 112 | 386 | 17.9 | 155 | 172 | 46.9 | 251 | 445 |
| 357 | SW 4/2 | 50.7H | 247 | 132 | >100H | ... | −50 | 22.4 | 192 | 122 | 52.8 | 112 | 137 |
| 358 | SW 4/4 | ... | ... | ... | ... | ... | ... | ... | ... | ... | ... | ... | ... |
| 359 | SW 4/5 | 34.7H | 241 | 456 | 69.7H | 257 | 936 | 18.5 | 199 | 283 | 48.0H | 110 | 622 |
| 360 | SW 4/6 | 33.0H | 240 | −75 | 66.2H | 256 | −153 | 18.4 | 199 | −47 | 47.4H | 110 | −106 |
| 361 | NE 1–2/1 | 23.7 | 350 | 223 | 23.5 | 353 | 220 | 23.3 | 359 | 220 | 24.1 | 346 | 224 |
| 362 | NE 1–2/2 | 31.9H | 21 | 200 | 58.7H | 60 | 369 | 29.9 | 5 | 192 | 42.8H | 314 | 263 |
| 363 | NE 6/1[a] | ... | ... | ... | ... | ... | ... | ... | ... | ... | ... | ... | ... |
| 364 | NE 6/4 | 22.4 | 327 | 250 | 22.1 | 328 | 246 | 19.3 | 350 | 214 | 41.9H | 63 | 457 |
| 365 | NE 6/4a | 20.3 | 351 | 197 | 20.1 | 355 | 194 | 20.1 | 359 | 194 | 20.4 | 350 | 197 |
| 366 | NE 6/5 | 26.6 | 313 | 281 | 25.6 | 316 | 267 | 19.4 | 344 | 204 | 44.6H | 66 | 463 |
| 367 | NE 6/6 | 36.2H | 307 | −264 | 38.7H | 305 | −269 | 22.9 | 349 | −171 | 48.0H | 63 | −345 |
| 368 | NE 6/8 | 32.4H | 313 | 331 | 31.0H | 317 | 304 | 23.0 | 350 | 237 | 46.4H | 62 | 465 |
| 369 | NE 6/9 | 26.4 | 310 | 194 | 25.7 | 312 | 185 | 18.6 | 341 | 136 | 44.7H | 68 | 322 |
| 370 | NE 6/10 | 19.1 | 340 | 241 | 18.8 | 343 | 236 | 18.1 | 355 | 227 | 19.1 | 340 | 241 |
| 371 | NE 6/P1 | 29.1 | 324 | 268 | 26.9 | 332 | 243 | 24.0 | 354 | 221 | 44.2H | 58 | 399 |
| 372 | NE 6/P2 | 37.4H | 302 | 244 | 43.5H | 298 | 269 | 21.5 | 346 | 146 | 48.7H | 66 | 314 |

NOTE.—Halo objects are shown with an "H" after the disk radius; $\theta$ is in degrees measured in the direction of rotation (counterclockwise) from the $+x$-axis of Fig. 1.

[a] NE 6/1 is an H II region (BA 685; Baade and Arp 1964).

Only the right-hand side depends on $i_i$, so that each planetary provides an unbiased estimate of the rotation rate. We can therefore estimate the expectation in equation (5) by the average over the $k$ planetaries:

$$v_c = \frac{1}{k} \sum_i \frac{v_i}{\alpha_i} - \mu \,. \tag{6}$$

We can estimate $\mu$ from the planetaries by asking that equation (6) give the same $v_c$ from the northeast planetaries as it does for the southwest planetaries. This implies $\mu = -290$, $-293$, $-294$, and $-295$ km s$^{-1}$ for the flat disk, Newton-Emerson, and Roberts, Whitehurst, and Henderson models, respectively. However, considering uncertainties due to noncircular motions and the small sample, especially on the northeast side, we adopt $\mu = -299$ km s$^{-1}$ (de Vaucouleurs, de Vaucouleurs, and Corwin 1976) as a better estimate. The individual values of $v_i/\alpha_i$ calculated using the flat model are shown in Figure 2, together with the H I and H II rotation curve from Roberts and Whitehurst (1975). Note that $v_i/\alpha_i$ is not necessarily the $\theta$ velocity of the planetary, since the contributions of $v_r$ and $v_z$ are unknown, and only the average is to be compared with the gas rotation curve. The implied $\theta$ velocity for all four models is given in Table 8.

### iii) *Separating Disk from Halo Objects*

The large majority of the planetaries center fairly well around the gas rotation curve, indicating that they are probably members of a disk population. M31-353, M31-357 (Newton-Emerson only), M31-360, and M31-366, however, have $v_i/\alpha_i$ of opposite sign to the rest of the disk. Their orbits are almost certainly not confined to the disk, and are strong evidence that the present sample includes both disk and halo objects. Except for these four, however, it is not clear how to tell one from the other, and the borderline is necessarily rather fuzzy. For disk membership we use the simple criteria that the implied $\theta$ velocity be positive (same sense of rotation as the rest of the disk), and that the disk projected radius $r_d$ be less than 30 kpc. The 30 kpc limit was adopted because an exponential fitted to the disk density due to all planetaries falls to near zero here, and because there is no evidence of a stellar disk beyond $\sim$27 kpc (Innanen *et al.* 1982). We experimented with a 25 kpc limit as well, and found only minor differences in the results. Of the three planetaries without velocities, SW 3/2 and 358 project to disk distances beyond 40 kpc for the flat, Newton-Emerson, and Henderson models, and are considered halo objects. SW 2/3 projects to 28 kpc for the flat and Newton-Emerson models. Its classification is uncertain and has therefore been neglected in our analysis. This left 12, 14, 3, and 19 planetaries in the halo for the flat, Newton-Emerson, Roberts-Whitehurst, and Henderson models, respectively.

### iv) *Rotation Rate and Velocity Dispersions*

We used equation (5) to find the rotation velocity of the planetaries. The results are given in Table 8. The flat and Newton-Emerson models give $220 \pm 12$ and $217 \pm 12$ km s$^{-1}$, respectively. Compare this with the H I and H II flat rotation curves. Roberts and Whitehurst found 228 km s$^{-1}$, Newton and Emerson found 232 km s$^{-1}$, and Haud, using all available velocity data with Henderson's model, found 232 km s$^{-1}$. We adopt 230 km s$^{-1}$ as the circular rotation speed beyond 15 kpc. This gives a marginally significant asymmetric drift of $\sim$14 km s$^{-1}$, about the same as the solar neighborhood value (Cahn and Wyatt 1978; Cudworth 1974) and suggests that the planetary nebula orbits are noncircular.

We used equation (1) to find a least-squares solution to the dispersions in the $r$ and $\theta$ directions. The $z$ dispersion, however, must be assumed. This is because the $z$ projection factor cos $i$ is very nearly the same for all planetaries, reducing the rank of the least-squares solution matrix to 2.

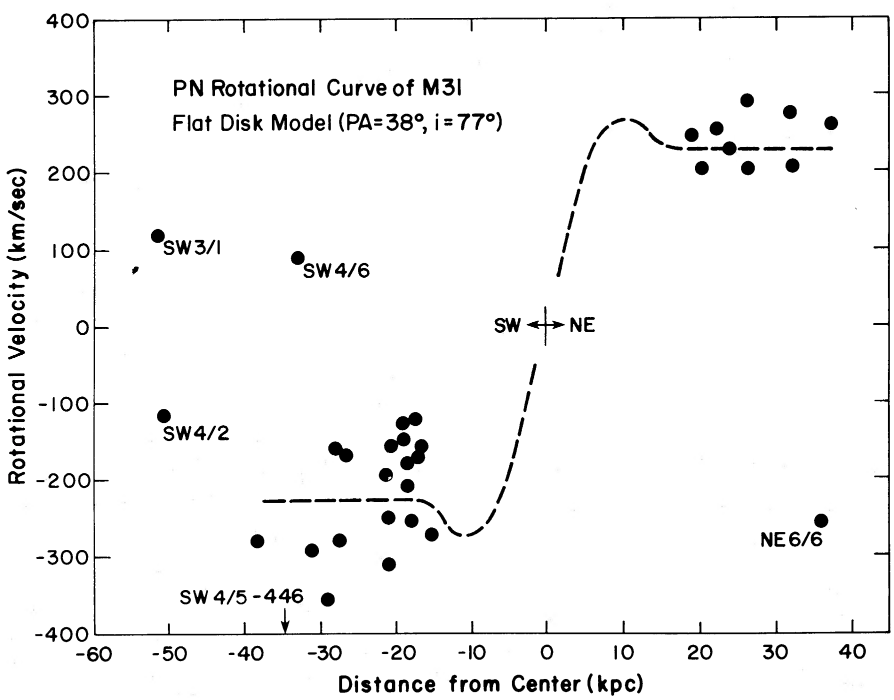


FIG. 2.—Dots are the rotation velocities of the planetaries inferred from their line-of-sight velocities if in circular orbits. The dotted curve is the composite H I and H II rotation curve from Roberts and Whitehurst (1975). Obvious halo objects are labeled.

Define the total dispersion for the $i$th planetary nebula as

$$\delta_i^2 \equiv (v_i - \mu - \alpha_i v_c)^2 . \tag{7}$$

Expanding this by using equation (1), taking an expectation along the $i$th line of sight, defining the dispersions as the expectations of the squared velocities in the $r$, $z$, and $\theta$ (after subtracting $v_c$) directions, and minimizing

$$\chi^2 = \sum_i [\delta_i^2 - E(\delta_i^2)]^2$$

with respect to $r$ and $\theta$ gives the dispersions

$$\sigma_\theta^2 = \left\{ \sum_k \beta_k^2 \sum_i \alpha_i^2 \left[ \delta_i^2 - \sigma_e^2 - \sigma_z^2 \sum_j (\alpha_i^2 \gamma_j^2) \right] - \sum_k \alpha_k^2 \beta_k^2 \sum_i \beta_i^2 \left[ \delta_i^2 - \sigma_e^2 - \sigma_z^2 \sum_j (\beta_i^2 \gamma_j^2) \right] \right\} \times \left[ \sum_i \alpha_i^4 \sum_i \beta_i^4 - \left( \sum_i \alpha_i^2 \beta_i^2 \right)^2 \right]^{-1} , \tag{8}$$

$$\sigma_r^2 = \left\{ \sum_k \alpha_k^2 \sum_i \alpha_i^2 \left[ \delta_i^2 - \sigma_e^2 - \sigma_z^2 \sum_j (\beta_i^2 \lambda_j^2) \right] - \sum_k \alpha_k^2 \beta_k^2 \sum_i \alpha_i^2 \left[ \delta_i^2 - \sigma_e^2 - \sigma_z^2 \sum_j (\alpha_i^2 \gamma_j)^2 \right] \right\} \times \left[ \sum_i \alpha_i^4 \sum_j \beta_j^4 - \left( \sum_i \alpha_i^2 \beta_i^2 \right)^2 \right]^{-1} . \tag{9}$$

The error in $\sigma_r$ and $\sigma_\theta$ is found from the individual error estimates of each term (cf. Table 9) by propagation of errors (Bevington 1969).

### v) *Thickness of the Disk*

Because M31's disk is not seen edge-on, the thickness of the disk planetary nebula distribution must be inferred. For a self-gravitating disk (van der Kruit and Freeman 1984), there is a simple relation between the velocity dispersion, the scale height in the $z$ direction, and the surface density of matter. We can estimate the $z$ velocity dispersion by using the $\theta$ dispersion and the assumed ratios $\sigma_r:\sigma_\theta:\sigma_z = 0.77:0.49:0.41$ from Wielen's (1977) isotropic diffusion theory and the observed solar neighborhood ratios (Gliese 1969; Oort 1965).

To obtain the surface mass density, we assume a self-gravitating, locally isothermal constant thickness (van der Kruit and Searle 1981*a*, *b*, 1982*a*, *b*), constant $M/L$ (van der Kruit 1981; Sancisi and Allen 1979) exponential disk, so that (Bahcall and Casertano 1985)

$$\rho(r, z) = \rho_0 e^{-r/h} \operatorname{sech}^2 (z/z_0) \tag{10}$$

TABLE 9

M31 DISPERSION ANALYSIS QUANTITIES

| Quantity | Value |
|---|---|
| H I disk rotation velocity | 232 km s$^{-1}$ |
| System velocity $\mu$ | −299 km s$^{-1}$ |
| Uncertainty in system velocity | 5 km s$^{-1}$ |
| Planetary nebula (PN) velocity error $\sigma_e$ | 10 km s$^{-1}$ |
| Uncertainty in PN velocity error | 4 km s$^{-1}$ |
| Disk PN $z$ velocity dispersion $\sigma_z$ | 30 km s$^{-1}$ |
| Uncertainty in $z$ velocity dispersion | 12 km s$^{-1}$ |
| Uncertainty in disk $\theta$ position of each PN | 24° |
| PN disk scale height $z_0$ | 3.0 kpc |
| Radial exponential density scale length | 4.6 kpc |

and

$$\alpha_z^2 = \pi G S(r) z_0 , \tag{11}$$

where $z_0$ is the scale height of the planetaries. The exponentially weighted mean radius of the planetaries is 17.8 kpc. We assume a mass distribution midway between a pure disk, given by Roberts and Whitehurst's (1975) Figure 16, and pure $r^{-2}$ halo and add the constraint that 60% of the total mass inside 23 kpc is due to the halo (van der Kruit and Freeman 1984) and obtain

$$S(17.8 \text{ kpc}) \approx 23 \ M_\odot \text{ pc}^{-2} . \tag{12}$$

Substituting this and $\sigma_z = 30$ km s$^{-1}$ in equation (11) gives a planetary nebulae disk scale height of 3.0 kpc—a fairly thick disk. The corresponding $\langle z^2 \rangle$ is 2.7 kpc. A Monte Carlo simulation placing the planetaries according to a Gaussian (0, $\langle z^2 \rangle$) distribution with the same sky positions gives a corresponding uncertainty in the $\theta$ coordinates of the planetaries in the disk of ~30° for the Henderson model and ~24° for the other three. This constitutes the dominant source of error in the $\sigma_r$, $\sigma_\theta$ calculation, leading to the large error bars shown in Figure 3. The dispersion in the radial direction is not meaningfully constrained, and only $\sigma_\theta$ can be directly estimated.

### vi) *Radial Distribution of Disk Planetaries*

In order to see what areas of the disk were sampled, we projected the plate fields shown in Figure 1 onto the four disk models (see Nolthenius 1984). The severe shadowing in the Henderson model and the previously discussed problems with the Roberts-Whitehurst model led to more uncertain disk projections. The Roberts-Whitehurst and Henderson disks are included in the calculations to follow, but the results should be viewed with caution.

We have divided the projected disk areas into rings and counted separately the areas sampled only by interference filter plates and the areas sampled by the slightly deeper GG 475 plates. We correct to a common depth by multiplying the areas sampled only by the interference filter plates by the factor 2/2.36, assuming roughly equal numbers of planetaries per unit magnitude interval (Jacoby 1980). The disk areas seen on all the plates are tabulated by radius bins in Table 10. Also tabulated is a guess of the error in the area measurements. We estimated this from the uncertainty due to shadowing, plus a contribution due to the thickness of the disk. M31's high inclination, uncertain warping, and the lack of direct extinction measurements make correcting the number of planetaries for extinction difficult. We have therefore made two simplifying assumptions: (1) the dust has circular symmetry about the galaxy, and (2) the H I gas-to-dust ratio is constant and about the same as in the solar neighborhood. For a flat disk, we can then correct for extinction by counting the $i$th planetary not once but $\eta_i$ times, where $\eta_i$ depends on the optical depth $\tau_i$ along the $i$th line of sight, shown in Figure 1 (see Appendix).

The surface density of planetaries is then just

$$S(r)_{\rm PN} = \frac{\sum_i \eta_i}{A(r)} , \tag{13}$$

where $A(r)$ is the sampled area of Table 10. Figure 4 shows $S(r)_{\rm PN}$ for each disk model, along with the best-fitting exponential curve with scale length $h = 4.6$ kpc. Using the best-fitting exponentials together with the exponential disk corresponding to 23 $M_\odot$ pc$^{-2}$ at $r = 17.8$ kpc gives an estimate of the

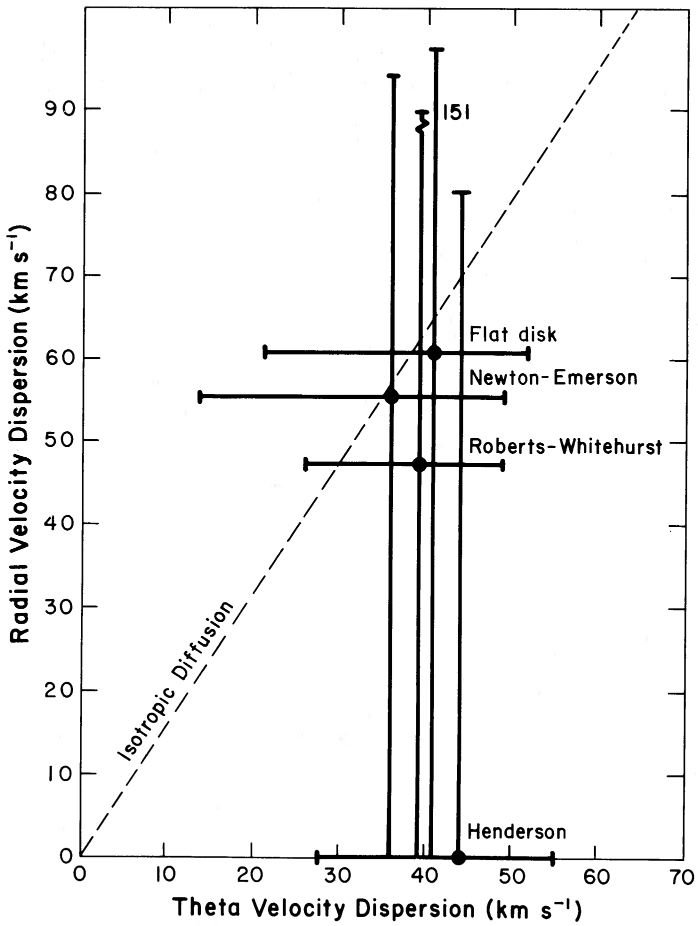


FIG. 3.—Least-squares solution for the velocity dispersions in the radial and azimuthal ($\theta$) direction from the disk planetaries using each of the published warp models. The high inclination and location of the plate fields allow only a very poor determination of $\sigma_r$. The dashed line shows the ratio $\sigma_r/\sigma_\theta$ predicted by isotropic diffusion theory.

mass specific density of disk planetaries, given in Table 11. The favored flat and Newton-Emerson disk models give $\sim(2–3) \times 10^{-8}$ planetary nebula per solar mass.

### b) *Halo Planetaries*

We have chosen to use only those planetaries which meet the halo criteria according to the flat disk model, for the following reasons, in addition to our earlier criticisms of the Roberts-Whitehurst and Henderson disk models: The Henderson model gives an improbably high fraction of halo objects, considering the kinematics (see Table 8). The flat model is simplest, and all halo objects selected are also selected by the favored Newton-Emerson model. Finally, any differences between the Newton-Emerson model and the flat model will be lost in the noise, because of the small sample size.

#### i) *Distribution*

The sky-projected density of planetaries in the halo was found by a method similar to that used for the disk. We measured the halo area (i.e., the area beyond disk radius $r_d = 30$ kpc) covered on each of the plates, corrected for differing plate sensitivity as before, and binned the areas into rings 4 kpc wide. These results are shown in Table 12. There is, however, an uncertainty in how to count the amount of halo area sampled. Halo objects could well be superposed on the areas where $r_d < 30$ kpc. Our criteria for halo selection would reveal these only if they had rotation sense opposite to that of the disk. The four planetaries with this rotation sense all fall outside $r_d = 30$ kpc. In fact, all the planetaries inside $r_d = 30$ kpc have $\theta$ velocities consistent with a disk population, so this problem is probably not severe. Nevertheless, this ambiguity is inherent in any necessarily uncertain way of separating disk from halo objects. Because of this, we will assume that only the $r_d > 30$ kpc areas are appropriate for finding the halo density law. Binning and counting the planetaries is straightforward, since $\tau = 0$ for all halo objects. The resulting density is plotted in Figure 5. Error bars correspond to 1 $\sigma$ Poisson noise.

With only a dozen objects to bin, it is obviously hard to say much about the form of the distribution. Correcting Crampton, Schade, and Chayer's (1984) "red" globular cluster $r^{1/4}$ law to a full population of 509 at 690 kpc gives an $r_e$ of 10.7 kpc. Using this same slope, the halo planetaries are best fitted by an $r^{1/4}$ law of the form

$$\log d(r)_{\rm PN} = 2.46 - 1.84 r^{1/4} \quad (D = 690 \text{ kpc}) . \qquad (14)$$

This is shown as a dotted line on Figure 5. It is nearly identical with the $\beta = 3.5$ power law.

A comparison with the Crampton, Schade, and Chayer (1984) catalog shows no planetaries within $5\langle\text{FWHM}\rangle = 10''$ of any known globulars. However, the cluster continuum in the off-band filter would make detection of planetary nebulae in globulars difficult.

TABLE 10

DISK AREA SAMPLED AND NUMBER OF PLANETARIES VERSUS RADIUS

| R (kpc) | AREA ($kpc^2$) Flat | Roberts-Whitehurst | Newson-Emerson | Henderson |
|---|---|---|---|---|
| 10–14 ........... | 0<br>0 (0)<br>0 (0) | 0<br>0 (0)<br>0 (0) | 0<br>0 (0)<br>0 (0) | 0<br>8 (0)<br>8 (0) |
| 14–18 ........... | 19<br>63 (4)<br>79 (4.52) | 24<br>51 (7)<br>73 (7.89) | 20<br>56 (4)<br>73 (4.51) | 0<br>56 (4)<br>56 (4.52) |
| 18–22 ........... | 52<br>190 (11)<br>233 (12.46) | 28<br>75 (17)<br>99 (18.18) | 61<br>190 (9)<br>242 (10.24) | 112<br>114 (10)<br>210 (11.35) |
| 22–26 ........... | 65<br>226 (2)<br>281 (2.08) | 0<br>47 (6)<br>47 (6.01) | 65<br>216 (6)<br>271 (6.32) | 94<br>201 (1)<br>283 (1.01) |
| 26–30 ........... | 0<br>336 (7)<br>336 (7.09) | 6<br>23 (3)<br>28 (3.07) | 27<br>329 (3)<br>362 (3.08) | 151<br>250 (2)<br>377 (2.07) |
| 30–34 ........... | 0<br>474 (3)<br>474 (3.0) | 11<br>13 (0)<br>22 (0) | 38<br>342 (0)<br>373 (0) | 143<br>369 (0)<br>489 (0) |
| 34–38 ........... | 90<br>266 (3)<br>344 (3.0) | 15<br>0 (0)<br>13 (0) | 40<br>266 (2)<br>302 (2.0) | 75<br>437 (0)<br>500 (0) |

NOTE.—For each bin, the first line gives the area covered only by the λ5007 interference filter plates, the second line gives the area covered on GG 475 plates, and the third line gives the total, corrected to the depth for the GG 475 plates (top 2.36 magnitudes of luminosity function). The estimated uncertainty in the areas is 5%, 12%, 15%, and 24%, for the Flat, Roberts-Whitehurst, Newton-Emerson, and Henderson models, respectively. In parentheses, the second line is the raw number $N$ of planetaries found in that bin. The third line is $N$ corrected for extinction by eq. (39).

ii) *Kinematics*

We assume that the velocity of each planetary is due to a rotation component with rotation axis perpendicular to the disk and an isotropic random velocity. This last is consistent with the dynamics of the globular cluster system of the Milky Way (Frenck and White 1980). The observed velocity of the $j$th planetary is then

$$v_j = \mu + v_c \cos\theta_j \sin i + \boldsymbol{v}_{r_j} \cdot \hat{\boldsymbol{s}} + \epsilon_j , \qquad (15)$$

where $\mu$ is the system velocity (assumed known), $i$ is the inclination of the disk, $v_c$ is the true rotation velocity of the halo planetary nebulae system, $\boldsymbol{v}_{r_j}$ is the random velocity, $\epsilon_j$ is the measurement error, and $\hat{s}$ is a unit vector along the line of sight. We estimate $v_c$ by taking the expectation along the $j$th line of sight. As we did for the disk, we replace the expectation over $v_j$ by an average over the $n$ sample planetaries, giving the estimated $v_c$ as

$$v_c = \frac{1}{n \sin i} \sum_j \frac{v_j - \mu}{E(\cos\theta_j)} . \qquad (16)$$

The expectations $E(\cos\theta_j)$ are an integration of all cos $\theta$'s along the $j$th line of sight, weighted by the density law of the planetaries, and are given in Table 13 for a $\beta = 3.5$ power law, where $\rho \propto r^{-\beta}$. Changing $\beta$ to 4.8 raises $E(\cos\theta_j)$ by only

TABLE 11

PLANETARIES PER UNIT DISK MASS

| Model (1) | Top 2.36 Magnitudes (2) | Top 8 Magnitudes[a] (3) | Top 8 Magnitudes[b] (4) | $\rho_{M31}/\rho_{LG}$ [c] (5) |
|---|---|---|---|---|
| Flat ........................ | $3.5 \times 10^{-9}$ | $3.2 \times 10^{-8}$ | $7.7 \times 10^{-8}$ | 0.15 |
| Newton-Emerson .......... | $2.7 \times 10^{-9}$ | $2.4 \times 10^{-8}$ | $5.8 \times 10^{-8}$ | 0.11 |
| Roberts-Whitehurst ........ | $9.6 \times 10^{-9}$ | $8.6 \times 10^{-8}$ | $2.1 \times 10^{-7}$ | 0.41 |
| Henderson .................. | $2.3 \times 10^{-9}$ | $2.0 \times 10^{-8}$ | $4.8 \times 10^{-8}$ | 0.10 |

NOTE.—Columns (2) and (3) give the mass specific density of planetaries in their outer disk, assuming that the disk density is given by $\rho_d = 1102 \exp(-r/4.6 \text{ kpc})\ M_\odot \text{ pc}^{-2}$.

[a] Derived from the observed number in the top 2.36 magnitudes using Jacoby's 1980 luminosity function for the Magellanic Clouds. This is the number used in calculating the last column.

[b] Derived from the observed number in the top 2.36 magnitudes using the solar neighborhood luminosity function (Jacoby 1980).

[c] Jacoby 1980 estimates the average mass specific density of planetaries in the top 8 magnitudes of the luminosity function for the Local Group as $\rho_{LG} = 2.1 \times 10^{-7}\ M_\odot^{-1}$.

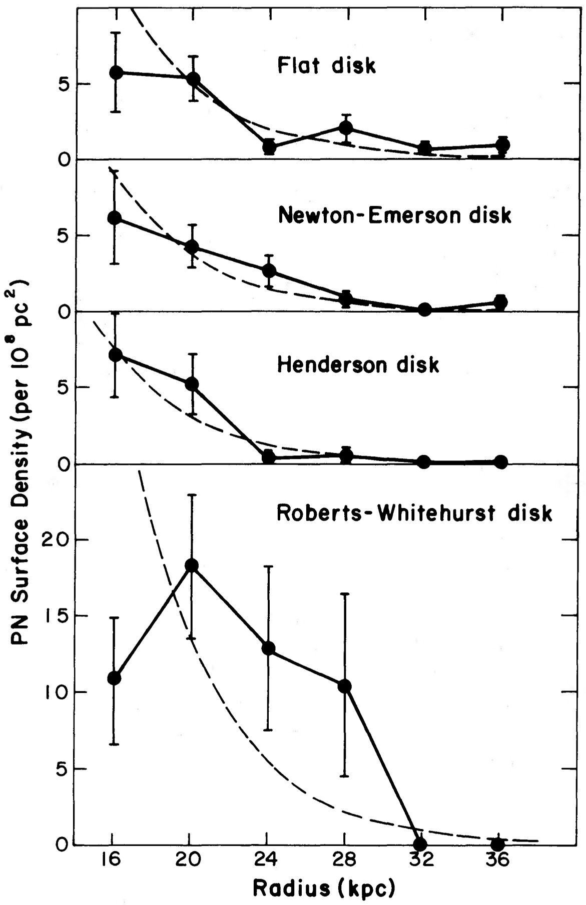


FIG. 4.—Surface density of planetary nebulae in the top 2.36 mag of the λ5007 luminosity function in the outer disk, assuming that each of the warp models includes all 34 planetaries. The dashed curves show the best-fitting exponential with scale length 4.6 kpc. These curves predict less than one disk planetary on the plates beyond disk radius 30 kpc, justifying the 30 kpc cutoff for disk membership. Including only planetaries considered disk members would zero the outer two bins in the flat model, and slightly lower the 20 and 24 kpc bins in the Roberts-Whitehurst fit. Error bars assume 1 σ Poisson noise.

TABLE 12

HALO PLANETARIES, BINNED BY RADIUS

| $R_{proj}$ (kpc) (1) | Number of Planetaries (2) | GG 475 Plates (3) | IF Plates Only (4) | Total Area ($kpc^2$) (5) |
|---|---|---|---|---|
| 15–19 | 4 | 62.9 | 3.8 | 66.1 |
| 19–23 | 4 | 87.6 | 15.3 | 100.5 |
| 23–27 | 0 | 41.7 | 4.7 | 45.8 |
| 27–31 | 1 | 59.4 | 0 | 59.4 |
| 31–35 | 0 | 32.6 | 21.7 | 51.1 |
| 35–39 | 0 | 0 | 34.4 | 29.1 |
| 39–43 | 0 | 0 | 33.8 | 28.5 |
| 43–47 | 0 | 0 | 5.9 | 5.0 |

NOTE.—Column (3) gives the area covered on GG 475 plates; col. (4) the area covered only by the λ5007 interference filter plates; and col. (5) the total area, corrected to the depth for the GG 475 plates (top 2.36 magnitudes of luminosity function).

TABLE 13

HALO PLANETARIES: POSITIONS, VELOCITIES, AND MEAN SKY PROJECTIONS

| Planetary | $x$ (kpc) | $y$ (kpc) | $R_{proj}$ (kpc) | $v$ (km $s^{-1}$)[a] | $E(\cos\theta)$[b] | $E(\cos^2\theta)$[b] |
|---|---|---|---|---|---|---|
| SW 3/1 | −19.1 | 10.8 | 21.9 | 36 | −0.901 | 0.825 |
| SW 3/A1 | −14.4 | 8.0 | 16.5 | −108 | −0.901 | 0.826 |
| SW 3/A2 | −15.4 | 6.1 | 16.5 | −145 | −0.911 | 0.841 |
| SW 4/2 | −19.7 | −10.5 | 22.3 | −50 | −0.903 | 0.828 |
| SW 4/5 | −16.6 | −6.9 | 17.9 | −212 | −0.910 | 0.840 |
| SW 4/6 | −16.5 | −6.4 | 17.7 | 36 | −0.911 | 0.842 |
| NE 1-2/2 | 29.7 | 2.6 | 29.8 | 182 | 0.922 | 0.858 |
| NE 6/6 | 21.6 | −6.5 | 22.5 | −153 | 0.915 | 0.849 |
| NE 6/8 | 22.1 | −5.3 | 22.7 | 220 | 0.916 | 0.848 |
| NE 6/P2 | 19.8 | −7.1 | 21.0 | 126 | 0.913 | 0.845 |
| SW 3/2 | −16.0 | 10.9 | 19.3 | ... | ... | ... |
| 358 | −13.4 | −9.0 | 16.1 | ... | ... | ... |

[a] Line-of-sight velocities, with respect to $\mu = -299$ km $s^{-1}$.

[b] Expectations of cos θ and $\cos^2\theta$ for a power-law space density with index of −3.5.

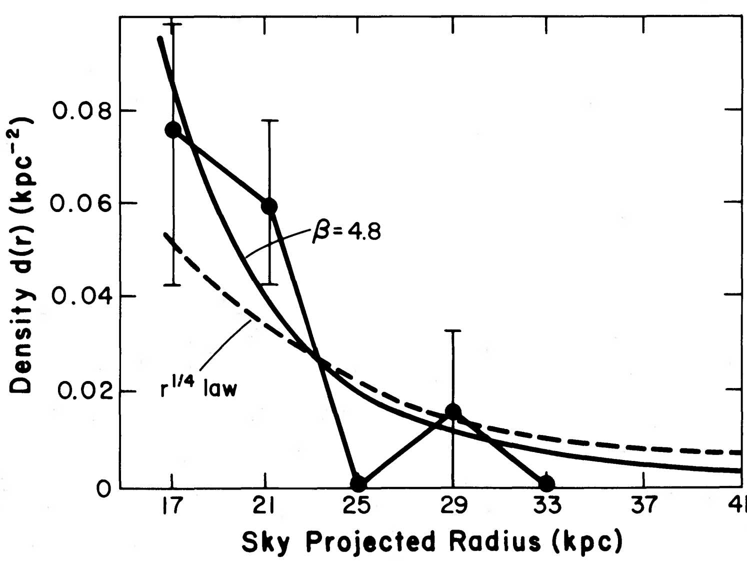


FIG. 5.—Sky-projected surface density of halo planetaries, using the halo objects selected by the flat disk model. Using the Newton-Emerson model would give only a minor change. Error bars are 1 σ. The best power-law fit to the planetaries is $\beta = 4.8$ and to the globular cluster distribution is $\beta = 3.5$. The dashed line is the best-fitting $r^{1/4}$ law for the planetaries, using the slope which best fits the globular cluster distribution, $r_e = 10.7$ kpc (Crampton, Schade, and Chayer 1984).

about 2%. Substituting these expectations in equation (16) gives a rotation velocity of $92 \pm 43$ km s$^{-1}$ in the same sense as the disk.

The line-of-sight velocity dispersion $\sigma_r^2$ is $E[(V_{r_j} \cdot \hat{s})^2]$, which becomes

$$\sigma_r^2 = \frac{1}{n} \sum_j (v_j - \mu)^2 - (v_c^2 \sin^2 i) \frac{1}{n} \sum_j E(\cos^2 \theta_j) - \sigma_e^2 . \quad (17)$$

$E(\cos^2 \theta_j)$ is calculated in the same way as $E(\cos \theta_j)$ and is given in Table 13. The resulting value of $\sigma_r$ is $116 \pm 48$ km s$^{-1}$. The error bars on $v_c$ and $\sigma_r$ are 1 $\sigma$ limits from a Monte Carlo simulation: we let the $v_i$ vary about their nominal values as a $(0, \sigma_r^2)$ Gaussian random variable, calculated $v_c$ and $\sigma_r$ for each trial, and found the dispersion about the nominal values. An isothermal oblate rotator with this dispersion and rotation rate would have flattening of $\epsilon = 0.39$ (Binney 1982).

### c) *Planetary-to-Light Ratio for Disk plus Halo*

The sum of $\eta_i$ for both disk and halo objects can be used to find the number of planetaries per unit light. Our Figure 1 sampled area, when projected onto de Vaucouleurs's (1958) isophotal map, encloses a total brightness of $m_B = 7.77$. Correcting $m_B$ for extinction in the Milky Way ($-0.26$ mag; Burstein and Heiles 1982 and Allen 1976) and internal extinction in M31 [$A(i) = -0.70 \log \sec (i = 77°) = -0.45$ mag], and making the $K$-correction for redshift ($= +0.10$ mag), the last two from de Vaucouleurs, de Vaucouleurs, and Corwin (1976), gives a total correction of

$$m_{\rm obs} - m_{\rm true} = 0.61 \quad (18)$$

for a true brightness of $m_B^* = 7.15$ and sampled luminosity of $1.02 \times 10^9\ L_\odot$. The number of planetaries (PN) per unit blue light is then

$$\frac{\rm PN}{L_{B\odot}} \text{(top 2.36 mag)} = \frac{\sum_i \eta_i}{1.02 \times 10^9\ L_\odot} = 3.83 \times 10^{-8}\ L_\odot^{-1} . \quad (19)$$

The $B - V$ of the outer disk is $+0.9$ (de Vaucouleurs 1958) and $M_{v\odot} = 4.83$ (Allen 1976), giving a ratio in visual light of $3.04 \times 10^{-8}\ L_\odot^{-1}$.

These values should be multiplied by 9 and 21 to correct to the top eight magnitudes (i.e., all planetaries; Jacoby 1980) using Jacoby's (1980) luminosity functions for planetaries in the Magellanic Clouds and the solar neighborhood, respectively. Hereafter, all extrapolations to the top eight magnitudes will use the Magellanic Clouds luminosity function. Corresponding estimates assuming the less reliable solar neighborhood luminosity function are a factor of 2.3 higher.

## IV. DISCUSSION

### a) *Disk Models*

While the planetary nebula data do not rule out any of the models considered here, we feel that the Newton-Emerson model is the most reasonable. The Roberts-Whitehurst model produces unrealistic sky-to-disk projection and should only be considered an H I velocity-fitting scheme (see Nolthenius 1984). All models give a higher halo population of planetaries than in the Galaxy, but Henderson's model in particular gives an unusually high fraction of halo objects, many with suspiciously disklike velocities. The flat model, on the other hand, conflicts with the pronounced asymmetry of the positions of the planetaries in Figure 1; 28 of the 37 planetaries are rotated clockwise away from the flat model major axis, the same direction as the H I and optical warps.

All models give $\sigma_\theta \sim 38$ km s$^{-1}$, implying $\sigma_r \sim 40$–60 km s$^{-1}$, which is sufficiently high to satisfy Toomre's (1964) local stability criteria.

Combining the measured asymmetric drift of the planetaries and Boltzmann's equation supplies another handle on the dispersions. For a self-gravitating disk with dispersions described by a Schwarzschild velocity ellipsoid with long axis parallel to the plane (Mihalas and Binney 1981) the relation can be written

$$v_c^2 - v_\theta^2 = -\sigma_r^2 \left[ \frac{\partial \ln \rho}{\partial \ln r} + \frac{\partial \ln \sigma_r^2}{\partial \ln r} + \left(1 - \frac{\sigma_\theta^2}{\sigma_r^2}\right) \right] , \quad (20)$$

where $v_c$ is the local circular velocity and $v_\theta$ is the stellar mean rotation velocity. The ratio $\sigma_r/\sigma_\theta$ is about $2^{1/2}$ for a flat rotation curve (Kormendy 1984). Averaging the values of $\sigma_\theta$ from Table 9 for the flat and Newton-Emerson models gives 38 km s$^{-1}$, which implies 53 km s$^{-1}$ for $\sigma_r$. From stability arguments (Mayor 1974) $\sigma_r^2$ should drop with radius. If $\sigma_r^2$ is everywhere close to the minimum stable value, it should drop exponentially, with scale length about equal to that for the density (Mayor 1974; Bahcall and Soneira 1980 for the Milky Way). The constancy of $z_0$ in edge-on spirals also suggests that the logarithmic gradients of $\rho$ and $\sigma_r^2$ should be nearly equal and constant (van der Kruit and Shostak 1983; van der Kruit and Searle 1981*a*, *b*, 1982*a*, *b*). Assuming that both $\rho$ and $\sigma_r^2$ drop as $\exp(-r/4.6)$ then implies a $v_\theta$ of $\sim 180$ km s$^{-1}$, rather lower than the 218 km s$^{-1}$ (average of flat and Newton-Emerson results) observed. Turning it around, a rotation rate of 218 km s$^{-1}$ implies a $\sigma_\theta$ of 21 km s$^{-1}$, about one standard deviation below the nominal value. Lowering $\sigma_z$ by the same factor implies a stellar disk scale height of 1.0 kpc. The small observed asymmetric drift therefore implies that the dispersions may be smaller and the stellar disk therefore thinner.

### b) *Disk Thickness*

Our estimated scale height $z_0$ of the M31 planetary nebula disk is surprisingly high: 1–3 kpc. This is considerably larger than the corresponding solar neighborhood value, where estimates range from 0.09 kpc (Cahn and Kaler 1971) to 0.16 kpc (Alloin, Cruz-Gonzalez, and Piembert 1976) to 0.26 kpc (Allen 1976) to 0.40 kpc (Blaauw 1965). Estimates of the local $\sigma_z$ are very uncertain because of the lack of planetaries near the Galactic poles. The published values are 20 km s$^{-1}$ (Wirtz 1922) and 27 km s$^{-1}$ (Oort 1928; this is probably an overestimate, since he assumes a spherical velocity ellipsoid). These, together with the fairly well determined local disk density of 75 $M_\odot$ pc$^{-2}$ (Bahcall 1984), imply $z_0 = 0.40$ and 0.72 kpc, respectively. The faint stars in the local disk also have a $z_0$ of 0.4 kpc (Bahcall and Soneira 1980).

Could our M31 scale height have been overestimated? The small asymmetric drift discussed above leads us in this direction. Also, since the calculated thickness depends directly on the velocity dispersions, counting the hotter halo objects as disk members could lead to an erroneously thicker disk. The halo planetary nebula density law (14) implies 8–10 halo members within the surveyed area which project to less than 30 kpc disk radius. It is remarkable, then, that all the planetaries here have velocities consistent with a disk population near the circular velocity. Eliminating the four planetaries with highest $|v_c - v_c^*|$ differences from the disk reduces the inferred $z_0$ by only 30%. This suggests that contamination is not severe, and also suggests that the halo density of planetaries may not rise as steeply toward the center as the bulge light profile implies. Alternatively, the Galactic scale height at $\sim 18$ kpc might be larger than it is locally. If the disk relaxation time is inversely proportional to the disk surface density, one expects an exponential increase in thickness with radius (Rohlfs 1983). Fitting this to real galaxies allows for up to a factor of $\sim 1.7$ increase, reducing the discrepancy somewhat. It is also possible that the $\sigma_z/\sigma_\theta$ ratio is lower than assumed. Hartwick (1985) finds $\sigma_r:\sigma_\theta:\sigma_z$ values of $141 \pm 23:106 \pm 23:56 \pm 30$ km s$^{-1}$ from 52 Galactic weak-line K giants with a scale height of $\sim 1$ kpc. Using these ratios in our analysis gives a $z_0$ of 1.3 kpc for the M31 planetaries.

A semithickness of 3–4 kpc is similar to the "thick disk" components seen in S0 galaxies (Burstein 1979). While the interpretation of thick disks is still uncertain (Bahcall and Kylafis 1985), they are traditionally characterized by a constant thickness of roughly 3–5 kpc, and a radial scale length longer than for the underlying thin disk. Thick disk candidates among spirals are NGC 891 (Freeman 1983) and the Milky Way (Gilmore and Reid 1983). Any "thick disk" present in M31 must be less than 1/15 as bright as those in Burstein's edge-on S0 sample (D. Burstein 1984, private communication). Since planetaries come from a fairly wide range of stellar ages, any thick disk indicated by the planetaries should also contain a general background of other intermediate and old stars. Whether such a background exists is not clear.

In our own Galaxy there is a stellar component with a thick disk intriguingly similar to that implied by the outer M31 planetaries. Ratnatunga and Freeman (1985) and Pier (1982, 1983) have found distant metal-poor K giants in high-latitude fields whose kinematics are consistent with nearly circular orbits within a $\sim 4:1$ flattened distribution (White 1985). It is not clear whether any planetary nebulae associated with this "thick disk" would be numerous enough to isolate as a separate population. Certainly the general Galactic outer halo population is quite small (cf. § IV*e*[i]).

From these considerations, it appears that the M31 outer disk planetaries occupy a thicker disk than those in the solar neighborhood, with $z_0$ in the neighborhood of 1–3 kpc, depending on assumptions. However, we caution that the disk thickness cannot be measured directly, and that, beyond the error bars quoted, these numbers are only as reliable as the model assumptions made (i.e., self-gravitating disk, $\sigma_z/\sigma_\theta$ ratio, mass distribution, and so on).

### c) Halo Planetaries

It is worth considering first whether the most bona fide of the nondisk planetaries, those rotating opposite to the disk, may be part of a Magellanic type of tidal stream (Mathewson, Clearly, and Murray 1974). Of course, it is easy to make a stream from just these planetaries, since they are selected by their countervelocity. What would be more convincing is to tie together these four planetaries with the unusual planetary M32-12, which has a velocity of approach 360 km s$^{-1}$ above the M31 system velocity. We can find no simple arc which will account for the positions and velocities of these five planetaries, or for these plus M32, which is the most likely cause of such a tidal stream.

The kinematics of the halo planetary nebulae in M31 appear to be similar to that of the globular cluster system. The net rotation of the planetaries is $92 \pm 43$ km s$^{-1}$, as compared with $80 \pm 28$ km s$^{-1}$ for the globulars (Huchra, Stauffer, and Van Speybroeck 1982). The velocity dispersions are $116 \pm 48$ km s$^{-1}$ for the planetaries and $\sim 130$ km s$^{-1}$ for the globulars (Huchra, Stauffer, and Van Speybroeck 1982).

How do the kinematics of the planetary nebulae compare with those of the bulge? Recent estimates of the bulge velocity dispersion are spread between $110 \pm 20$ km s$^{-1}$ (Morton, Andereck, and Bernard 1977) and 180 km s$^{-1}$ (Schechter and Gunn 1979). Lawrie (1978) found 157 km s$^{-1}$ from 42 planetary nebulae inside $r = 0.2$ kpc. The rotation curve rises more or less linearly to about 50 km s$^{-1}$ at 0.4 kpc, where the data stop. The value of $M/L_B$ corresponding to the dispersions above is 3–7 in solar units, a little lower than that for planetary nebula progenitors (but gas and dust could reduce the difference), and a little higher than that for globular clusters ($M/L \approx 2$).

Our sample of halo planetaries is too small to compare their space distribution with that of the bulge or globular clusters. From these results it appears equally likely that the field halo (as revealed by the halo planetaries) is an extension of the bulge, or associated with the globular cluster population. A more sensitive comparison will have to await a planned complete survey of M31.

The dispersion of the planetaries only drops from $\sim 150$ km s$^{-1}$ in the central bulge to $\sim 110$ at $\sim 22$ kpc. This argues against their being on highly radial orbits, especially if the appropriate effective radius is as small as 2.7 kpc. In fact the dispersion in an $r^{1/4}$ distribution with isotropic orbits should drop this much in only about $\sim 1 r_e$ (Merritt 1985). Even considering the scanty data, this is perhaps additional evidence for a massive halo less centrally condensed than the visible galaxy.

All of these derived properties of the M31 planetary nebulae are summarized in Table 14.

### d) Total Planetary Nebula Populations in M31 and the Milky Way

#### i) Spheroid

On the basis of the solar neighborhood disk planetary nebula population density, virtually all of Isaacman's (1983) Galactic center planetaries are bulge objects. Assuming that the top eight magnitudes of the H$\alpha$ luminosity function defines all planetaries, we have fitted an $r^{1/4}$ law to his data:

$$\log d = 4.92 - 3.08 r^{1/4} , \tag{21}$$

with $r$ in kpc and $d$ in projected kpc$^{-2}$, giving a total Milky Way bulge population of 1600. Of these, 280 should lie beyond 5 kpc. This is $\sim 8$–15 times the estimated number of halo planetaries (Cahn and Wyatt 1976, using Cudworth 1974 distance scale), and shows that, even considering the rather uncertain corrections in Isaacson's population estimate, there seems no need to invoke a separate halo distribution (e.g., distributed as the globulars) to account for observed Galactic halo planetaries. In fact, the surprise is that there are not more bulge planetaries in the solar neighborhood. This is compounded by the fact that the inner bulge planetaries are expected to live only $\sim 5000$ yr before ram pressure disperses them—a factor of 5 or so less than solar neighborhood lifetime estimates (Isaacman 1983).

This suggests that the appropriate effective radius for estimating the M31 spheroidal planetary nebula population is that of the bulge: 2.7 kpc. The corresponding density-law fit to

TABLE 14

SUMMARY OF DERIVED M31 PLANETARY NEBULA RESULTS

A. DISK PLANETARIES

| Quantity | Flat | Newton-Emerson | Roberts-Whitehurst | Henderson |
|---|---|---|---|---|
| Rotation velocity ($km\ s^{-1}$) ......... | $220 \pm 12$ | $217 \pm 12$ | $192 \pm 8$ | $195 \pm 11$ |
| Velocity dispersion in $r$ ($km\ s^{-1}$) ..... | $61^{+36}_{-61}$ | $56^{+39}_{-56}$ | $48^{+103}_{-48}$ | $0^{+80}_{-0}$ |
| Velocity dispersion in $\theta$ ($km\ s^{-1}$) .... | $41^{+13}_{-19}$ | $36^{+13}_{-22}$ | $39^{+10}_{-13}$ | $44^{+12}_{-16}$ |
| Density (PN $M_\odot^{-1}$) inside 30 kpc disk radius ...... | $3.5 \times 10^{-9}$ | $2.7 \times 10^{-9}$ | $9.6 \times 10^{-9}$ | $2.3 \times 10^{-9}$ |
| Fraction of PNs inside 30 kpc disk radius ...... | 0.67 | 0.61 | 1.00 | 0.47 |
| Scale height $\langle z^2 \rangle^{1/2}$ .......... | $3.4^{+0.7}_{-1.9}$ | $2.7^{+0.7}_{-1.6}$ | $3.2^{+0.5}_{-1.3}$ | $3.9^{+0.7}_{-1.9}$ |

B. HALO PLANETARIES

| Quantity | Value |
|---|---|
| Rotation velocity ($km\ s^{-1}$) .......................... | $92 \pm 43$ |
| Line-of-sight random velocity dispersion ($km\ s^{-1}$) ........................................... | $116 \pm 48$ |
| Sky-projected density law ($d$ in PN $kpc^{-2}$, $r$ in kpc) ......................... | $\log d = 2.46 - 1.84 r^{1/4}$ |
| Flattening of PN halo, $(b - a)/a$ .................... | 0.39 |
| Ratio of total PN population (top 8 magnitudes) to total globular cluster population ............. | 0.69 |

the halo planetary data of Figure 5 is then

$$\log d = 4.18 - 2.60 r^{1/4} \tag{22}$$

for a total spheroidal component population of 10,000. Assuming that the planetaries are distributed as the globular clusters gives the density law of equation (14) and a spheroidal population of 3100. These can be compared with the results of Ford and Jacoby (1978*a*). They estimate 66 planetaries within the top three magnitudes in an integrated apparent brightness of $m_B = 8.37$, essentially all due to the bulge. The total spheroidal component magnitude is $m_B = 5.91$ from de Vaucouleurs (1958), giving a spheroidal population (corrected to the top eight magnitudes) of 4800. The Ford and Jacoby result thus falls between our estimates using the bulge $r_e$ and the globular cluster $r_e$. The total M31 spheroidal population is then about 3–4 times the Milky Way value, adding to the evidence that M31 has a more massive spheroid and earlier Hubble type than the Milky Way.

ii) *Disk*

We estimate the disk population of planetaries by averaging the exponential fits to the Newton-Emerson and flat disk models in Figure 4. Inside 10 kpc, the disk light drops steeply to zero at the nucleus (de Vaucouleurs 1958). We therefore integrate only beyond 5 kpc, giving 300 planetaries in the top 2.36 magnitudes and 2700 total.

For the Galaxy, Cahn and Wyatt (1976) estimate that the solar neighborhood surface density of planetaries is $19 \pm 2$ $kpc^{-2}$, using Seaton's (1968) distance scale. We prefer the Cudworth (1974) scale for a variety of reasons (see Jacoby 1980, p. 16). On this scale, the most luminous known planetaries in M31 and the Galaxy are of equal brightness. Using the Cudworth scale the local density drops by a factor of 2.7 from Cahn and Wyatt's estimate. Assuming an exponential distribution from 3 to 30 kpc with scale length 3–5 kpc gives a total of 5000 planetaries in the disk, about the same as in M31.

While the total populations appear similar, the mass specific densities do not. Using 23 $M_\odot$ $pc^{-2}$ at 17.8 kpc distance, the M31 outer disk planetary nebula–to–mass ratio is $2.7 \times 10^{-8}$ $M_\odot^{-1}$. The corresponding ratio in the solar neighborhood is a factor of 3.5 larger—$9.3 \times 10^{-8}$ $M_\odot^{-1}$—again assuming the Cahn and Wyatt (1976) planetary nebula density corrected to the Cudworth distance scale, and 75 $M_\odot$ $pc^{-2}$ from Bahcall (1984). It is a factor of 8 smaller than the average for the Local Group (Jacoby 1980). It is unlikely that the associated uncertainties could remove this difference. Certainly if the outer disk mass were a factor of 8 lower, the planetaries would not be gravitationally confined to a disk. It is possible that the planetary nebula formation efficiency is lower in the outer disk. Fall and Efstathiou (1980) have suggested that spiral disks have edges corresponding to those radii at which the shear due to differential rotation becomes large enough to overcome self-gravity in the primordial disk, thus inhibiting star formation. The M31 disk does show a slight color gradient, being redder in the outer regions (de Vaucouleurs 1958). If this reflects a higher fraction of low-mass stars, it may mean that the initial mass function in the outer disk favors stars less massive than planetary nebula progenitors. If this is true, the outer disk may underrepresent the inner disk, leading to an underestimate of the total disk population of planetary nebulae.

The planetary-to-luminosity ratio is also low. The total (disk and halo) planetary nebula–to–luminosity ratio is $2.8 \times 10^{-7}$ $L_\odot^{-1}$ in blue light and $2.3 \times 10^{-7}$ $L_\odot^{-1}$ in visual light. However, in these outer regions nearly all of the light is due to the disk, as shown by the highly flattened isophotes (de Vaucouleurs 1958). Dividing the disk planetaries by the total light gives a planetary-to-light ratio of $1.7 \times 10^{-7}$ $L_\odot^{-1}$. This is only 28% of the Local Group average ($6.1 \times 10^{-7}$; Jacoby 1980), 55% of the solar neighborhood value, averaged through the thickness of the disk ($3.08 \times 10^{-7}$; Cahn and Wyatt 1976 on Cudworth scale and de Vaucouleurs and Pence 1978), and 20% of the value from the central M31 bulge ($8.6 \times 10^{-7}$; Ford and Jacoby 1978*a*). The discrepancy with the Local Group average and the inner bulge probably reflects stellar population differences. It is hard to judge the factor of 2 difference with the solar neighborhood ratio. Within the uncertainties, they may agree. On the other hand, adopting the Seaton distance scale will increase the difference by another factor of 3.

iii) *Total* (*Disk plus Spheroid*) *Populations*

It is probably safest to add the disk and halo contributions separately, rather than assuming a constant PN $M_\odot^{-1}$ or PN $L_\odot^{-1}$ ratio valid for both. For the reasons given above, the disk population may be underestimated, and $\sim 2700$ is perhaps a lower limit. Adding in the spheroid gives about 6000–12,000, depending on $r_e$. If the M31 PN $M_\odot^{-1}$ ratio throughout most of the disk is similar to that in the solar neighborhood, the disk population may be about 9000 and the total population 12,000–19,000.

Using the riskier procedure of assuming the same planetary-to-luminosity ratio for disk and halo gives 8000 from the outer region analysis presented here, and 20,000 from the inner bulge results of Ford and Jacoby (1978*a*).

Keep in mind that the halo population may be slightly overestimated (less than a factor of 2?) because of the lack of obvious halo objects at $r_{\rm disk} < 30$ kpc, and that the disk population may be underestimated, because the large mass specific density difference compared with that for the solar neighborhood suggests that the outer disk may not represent the inner disk.

All of these results should be compared with the Milky Way total of about 7000. Other Milky Way population estimates are generally in this area, but occasionally they range up to $38{,}000 \pm 12{,}000$ (Cahn and Wyatt 1976) or even higher. We have tried to standardize the best estimates by making uniform assumptions (e.g., $r^{1/4}$ law, Jacoby luminosity functions, to top eight magnitudes) and correcting other published results to bring them in line with these assumptions. We conclude that the total population of planetary nebulae in M31 is 1–2 times that in the Milky Way, the difference being due to a higher M31 spheroid population.

All estimates in this section are summarized in Table 15.

### *e) Planetary Nebula Contribution to Disk* H I

At 20 kpc, the disk and halo planetary nebula density is $0.045 \pm 0.035 = 0.08$ kpc$^{-2}$ (average of flat and Newton-Emerson disk curves from Fig. 4, and $r^{1/4}$ halo fit from Fig. 5) in the top 2.36 magnitudes of the $\lambda5007$ luminosity function. This corresponds to 0.104 kpc$^{-2}$ in the top three magnitudes. Assuming a lifetime within three magnitudes of the maximum of 14,700 years and 0.5 $M_\odot$ lost per star (Ford and Jacoby 1978*a*) gives 0.036 $M_\odot$ pc$^{-2}$ of reprocessed gas over $10^{10}$ yr. Supernovae contribute a similar amount. Together planetary nebulae and supernovae have contributed only 5% of the H I disk density (Roberts and Whitehurst 1975) and suggest either that the PN rate was much higher in the past or that most of the outer disk gas is unprocessed.

TABLE 15

Total Planetary Nebula Populations in M31 and the Milky Way

A. M31

| Population | $n(8)$[a] MC | SN |
|---|---|---|
| Disk | 2700 | 6300 |
| Spheroid (this study): | | |
| $r_e = 2.7$ kpc | 10000 | 23300 |
| $r_e = 10.7$ kpc | 3100 | 7200 |
| Spheroid (by PN $L_\odot^{-1}$ ratio; Ford and Jacoby 1978*a* inner bulge results) | 4500 | 11000 |
| Total, adding disk and $r_e = 2.7$ spheroid | 12700 | 29600 |
| Total (by PN $L_\odot^{-1}$ ratio; outer regions) | 8000 | 18700 |
| Total (by PN $L_\odot^{-1}$ ratio; Ford and Jacoby 1978*a*, inner bulge results) | 20000 | 46700 |

B. Milky Way

| Population | $n(8)$ | Source |
|---|---|---|
| Disk | 5000 | Cahn and Wyatt 1976 and § IV*e*(ii) |
| Spheroid | 1600 | Isaacman 1983 and § IV*e*(i) |
| Spheroid | 30–60 | Extrapolation from local halo PNs (Cahn and Wyatt 1976), assumed distributed as globular cluster population |

[a] Extrapolating from top 2.36 to top 8 magnitudes using Magellanic Clouds or solar neighborhood luminosity functions $n(m)$ (see Jacoby 1980).

## V. SUMMARY

The conclusions of this study are summarized below.

1. The $\theta$ velocity dispersion of the old disk stars in M31, as represented by the planetary nebulae, is $\sim 38 \pm 15$ km s$^{-1}$ at $\langle r \rangle = 18$ kpc. With reasonable dynamical assumptions this yields a disk scale height $z_0$ of 1.0–3.0 kpc, a factor of 5–15 higher than the solar neighborhood planetaries. This may indicate an increasing disk thickness with $r$, or a "thick disk" component. The disk is hot enough to satisfy Toomre's (1964) local stability criterion.
2. The exponential scale length of the M31 disk planetary nebula distribution is consistent with that for the overall disk light.
3. The planetary-to-disk mass ratio in M31 is about a factor of 3.5 lower than in the solar neighborhood.
4. Approximately 12 of the 37 planetaries are halo members. Their rotation and velocity dispersion agree well with that for the globular cluster system, which partially overlaps the sampled area (on the small-$r$ side).
5. None of the disk or halo planetaries are in known globular clusters.
6. The spheroidal population of planetaries is about 3000–10,000, depending on $r_e$, a factor of 2–6 times the Milky Way value. This supports the idea that M31 has a more prominent spheroid and is probably of earlier Hubble type than the Milky Way.
7. The disk population is about 3000, comparable to or a little lower than the Milky Way value. This outer disk estimate may underestimate the total disk population, since the PN $M_\odot^{-1}$ ratio here may be lower than in the inner disk.
8. A reasonable overall estimate of the total planetary nebula population in M31 is about 12,000. This is roughly twice the Milky Way population. A probable lower limit is 6000.

This work was part of R. A. N.'s dissertation at UCLA; thanks go to the Office of Academic Computing for a continuing grant of computer resources. I also thank Robin Ciardullo and the Space Telescope Science Institute for their hospitality during a brief but productive visit in the summer of 1984; the staff of Steward Observatory, who assisted in the final preparation of this paper; and Simon White for a critical reading of the manuscript. We are grateful to Dr. David Jenner for invaluable help in doing the photographic survey of M31 and in measuring the radial velocities of the planetary nebulae. We wish to thank Eric Eason for blinking the plates and reducing the radial velocity measurements. Part of this work was supported under National Science Foundation grant AST-8352062.

## APPENDIX

## CORRECTING THE NUMBER OF PLANETARIES FOR EXTINCTION

Using the absorption in $\lambda 5007$ given by Allen (1976) and equations (4), (5), and (6) from Ford and Jacoby (1978*a*) together with Roberts's (1966) integrated brightness temperature contour map of M31, we have estimated $\tau(\lambda 5007)$ and plotted it on Figure 1.

We found $\eta_i$ as follows. Jacoby's (1980) planetary nebula luminosity function shows that the number per unit magnitude is approximately constant over the top three magnitudes. Let $m_b$ be the brightest planetary and $m_f$ be the faintest detectable on the GG 475 plates. Then if a planetary in the top 2.36 magnitudes of the luminosity function $n(m)$ is seen through optical depth $\tau(\sim$ magnitudes of extinction), the probability $p$ of detecting it is reduced to

$$p_i = \frac{m_f - m_b - \tau_i}{m_f - m_b}, \tag{A1}$$

and $\eta_i$ for that planetary is just the reciprocal of $p_i$.

In general, one has only an upper limit to $\tau$, since the planetary could be anywhere within the obscuring layer. However, the planetary nebula disk seems to be significantly thicker than the H I disk (and presumably the dust layer): 6 kpc versus $\sim$0.5–2 kpc (depending on the source). We will therefore assume that the planetary is seen either through the $\tau$ of Figure 1 (far side of dust) or through $\tau = 0$ (near side). Then the probability of finding the planetary on the far side is

$$p_f = \frac{\int_{m_f-\tau}^{m_b} n(m)dm}{\int_{m_f-\tau}^{m_b} n(m)dm + \int_{m_f}^{m_b} n(m)dm} = \frac{2.36 - \tau}{4.7 - \tau}, \tag{A2}$$

where $m_f - m_b = 2.36$. The probability that the planetary is on the near side is just $p_n = 1 - p_f$. Then $\eta$ is given by

$$\eta_i = p_{n_i} + \frac{p_{f_i}}{p_i} = \frac{4.7}{4.7 - \tau_i}. \tag{A3}$$

The sum of $\eta_i$ for each bin is given in Table 5. Notice that the correction for extinction is relatively small.

## REFERENCES


Allen, C. W. 1976, *Astrophysical Quantities* (London: Athlone).
Alloin, D., Cruz-Gonzalez, C., and Peimbert, M. 1976, *Ap. J.*, **205**, 74.
Arp, H. 1964, *Ap. J.*, **139**, 1045.
Baade, W. 1963, in *Evolution of Stars and Galaxies* (Cambridge: Harvard University Press), p. 73.
Baade, W., and Arp, H. 1964, *Ap. J.*, **139**, 1027.
Bahcall, J. N. 1984, *Ap. J.*, **276**, 156.
Bahcall, J. N., and Casertano, S. 1985, *Ap. J. (Letters)*, **293**, L7.
Bahcall, J. N., and Kylafis, N. D. 1985, *Ap. J.*, **288**, 252.
Bahcall, J. N., and Soneira, R. M. 1980, *Ap. J. Suppl.*, **44**, 73.
Bevington, P. R. 1969, *Data Reduction and Error Analysis for the Physical Sciences* (New York: McGraw-Hill).
Binney, J. 1982, *Ann. Rev. Astr. Ap.*, **20**, 399.
Blaauw, A. 1965, in *Stars and Stellar Systems*, Vol. **5**, *Galactic Structure*, ed. A. Blaauw and M. Schmidt (Chicago: University of Chicago Press), p. 435.
Brinks, E., and Burton, W. B. 1984, *Astr. Ap.*, **141**, 195.
Burstein, D. 1979, *Ap. J.*, **234**, 829.
Burstein, D., and Heiles, C. 1982, *A.J.*, **87**, 1165.
Cahn, J. H., and Kaler, J. B. 1971, *Ap. J. Suppl.*, **189**, 319.
Cahn, J. H., and Wyatt, S. P. 1976, *Ap. J.*, **210**, 508.
———. 1978, in *IAU Symposium 76, Planetary Nebulae Observations and Theory*, ed. Y. Terzian (Dordrecht: Reidel), p. 3.
Crampton, D., Schade, D., and Chayer, P. 1984, DAO preprint.
Cudworth, K. M. 1974, *A.J.*, **79**, 1384.
de Vaucouleurs, G. 1958, *Ap. J.*, **128**, 465.
de Vaucouleurs, G., de Vaucouleurs, A., and Corwin, H. 1976, *Second Reference Catalogue of Bright Galaxies* (Austin: University of Texas Press) (RC2).
de Vaucouleurs, G., and Pence, W. D. 1978, *Ap. J.*, **83**, 1163.
Emerson, D. T., and Newton, K. 1978, in *IAU Symposium 77, Structure and Properties of Nearby Galaxies*, ed. E. M. Berkhuijsen and R. Wielebinski (Dordrecht: Reidel), p. 183.
Fall, S. M., and Efstathiou, G. 1980, *M.N.R.A.S.*, **193**, 189.
Ford, H. C., and Jacoby, G. 1978*a*, *Ap. J.*, **219**, 437 (Paper V).
———. 1978*b*, *Ap. J. Suppl.*, **38**, 351 (Paper VIII).
Ford, H. C., Jacoby, G., and Jenner, D. C. 1977, *Ap. J.*, **213**, 18 (FJJ).
Ford, H. C., and Jenner, D. C. 1975, *Ap. J.*, **219**, 437.
Freeman, K. C. 1983, in *IAU Symposium 106, The Milky Way Galaxy*, ed. H. van Woerden (Dordrecht: Reidel).
Frenck, C., and White, S. D. M. 1980, *M.N.R.A.S.*, **193**, 295.
Gilmore, G., and Reid, N. 1983, *M.N.R.A.S.*, **202**, 1025.
Gliese, W. 1969, *Veröff. Astr. Rechen-Inst. Heidelberg*, No. 22.
Hartwick, F. D. A. 1985, unpublished.
Haud, U. 1981, *Ap. Space Sci.*, **76**, 477.
Henderson, A. P. 1979, *Astr. Ap.*, **75**, 311.
Huchra, J., Stauffer, J., and Van Speybroeck, L. 1982, *Ap. J. (Letters)*, **259**, L57.
Innanen, K. A., Kamper, K. W., Papp, K. A., and van den Bergh, S. 1982, *Ap. J.*, **254**, 515.
Isaacman, R. 1983, in *IAU Symposium 103, Planetary Nebulae*, ed. D. R. Flower (Dordrecht: Reidel), p. 415.
Jacoby, G. H. 1980, *Ap. J. Suppl.*, **42**, 1.
Kormendy, J. 1984, *Ap. J.*, **286**, 116.
Lawrie, D. G. 1978, Ph.D. thesis, University of California, Los Angeles.
Lawrie, D. G., and Ford, H. C. 1982, *Ap. J.*, **156**, 112 (Paper IX).
Mathewson, D. S., Clearly, M. N., and Murray, J. D. 1974, in *IAU Symposium 58, Formation and Dynamics of Galaxies*, ed. J. R. Shakeshaft (Dordrecht: Reidel), p. 367.
Mayor, M. 1974, *Astr. Ap.*, **32**, 321.
Merritt, D. 1985, *A.J.*, **90**, 1027.
Mihalas, D., and Binney, J. 1981, *Galactic Astronomy: Structure and Kinematics* (2d ed.; San Francisco: Freeman).
Miller, J. S., Robinson, L. B., and Wampler, E. J. 1976, *Adv. Electronics Electron Phys.*, **40**, 693.
Morton, D. C., Andereck, C. D., and Bernard, D. A. 1977, *Ap. J.*, **212**, 13.
Newton, K., and Emerson, D. T. 1977, *M.N.R.A.S.*, **181**, 573.
Nolthenius, R. 1984, Ph.D. thesis, University of California, Los Angeles.
Nolthenius, R., and Ford, H. C. 1986, *Ap. J.*, **305**, 600.
Oort, J. H. 1928, *Bull. Astr. Inst. Netherlands*, **4**, 269.
———. 1965, in *Stars and Stellar Systems*, Vol. **5**, *Galactic Structure*, ed. A. Blaauw and M. Schmidt (Chicago: University of Chicago Press), p. 483.
Pier, J. R. 1982, *A.J.*, **87**, 1515.
———. 1983, *Ap. J. Suppl.*, **53**, 791.
Ratnatunga, K. U., and Freeman, K. C. 1985, *Ap. J.*, **291**, 260.
Roberts, M. S. 1966, *Ap. J.*, **144**, 639.
Roberts, M. S., and Whitehurst, R. N. 1975, *Ap. J.*, **201**, 327.
Robinson, L. B., and Wampler, E. J. 1972, *Pub. A.S.P.*, **84**, 161.
———. 1973, in *Astronomical Observations with Television-Type Sensors*, ed. J. W. Glaspey and G. A. H. Walker (Vancouver: University of British Columbia), p. 69.
Rohlfs, K. 1983, in *IAU Symposium 100, Internal Kinematics and Dynamics of Galaxies*, ed. E. Athanassoula (Dordrecht: Reidel), p. 77.
Sancisi, R., and Allen, R. J. 1979, *Astr. Ap.*, **74**, 73.
Schechter, P., and Gunn, J. E. 1979, *Ap. J.*, **229**, 472.
Schneider, S., Terzian, Y., Purgathofer, A., and Perinotto, M. 1983, *Ap. J. Suppl.*, **52**, 399.
Seaton, M. J. 1968, *Ap. Letters*, **2**, 55.
Toomre, A. 1964, *Ap. J.*, **139**, 1217.
van den Bergh, S. 1969, *Ap. J. Suppl.*, **19**, 145.
van der Kruit, P. C. 1981, *Astr. Ap.*, **99**, 298.
van der Kruit, P. C., and Freeman, K. C. 1984, *Ap. J.*, **278**, 81.
van der Kruit, P. C., and Searle, L. 1981*a*, *Astr. Ap.*, **95**, 105.

van der Kruit, P. C., and Searle, L. 1981*b*, *Astr. Ap.*, **95**, 116.
———. 1982*a*, *Astr. Ap.*, **110**, 61.
———. 1982*b*, *Astr. Ap.*, **110**, 79.
van der Kruit, P. C., and Shostak, G. S. 1983, in *IAU Symposium 100, Internal Kinematics and Dynamics of Galaxies*, ed. E. Athanassoula (Dordrecht: Reidel), p. 69.
White, S. D. M. 1985, *Ap. J.* (*Letters*), **294**, L99.
Whitehurst, R. N., Roberts, M. S., and Cram, T. R. 1978, in *IAU Symposium 77, Structure and Properties of Nearby Galaxies*, ed. E. M. Berkhuijsen and R. Wielebinski (Dordrecht: Reidel), p. 175.
Weilen, R. 1977, *Astr. Ap.*, **60**, 263.
Wirtz, C. 1922, *Astr. Nach.*, **215**, 281.
Wyse, R. F. G., and Jones, B. J. T. 1983, in *IAU Symposium 100, Internal Kinematics and Dynamics of Galaxies*, ed. E. Athanassoula (Dordrecht: Reidel), p. 389.

HOLLAND C. FORD: Space Telescope Science Institute, Homewood Campus, Baltimore, MD 21218

RICHARD NOLTHENIUS: Board of Studies in Astronomy and Astrophysics, University of California, Santa Cruz, CA 95064